NASA Technical Paper 1697

Experimental Investigation of the Radiation of Sound From an Unflanged Duct and a Bellmouth, Including the Flow Effect

Jean-Michel Ville and Richard J. Silcox

AUGUST 1980

NASA

NASA Technical Paper 1697

Experimental Investigation of the Radiation of Sound From an Unflanged Duct and a Bellmouth, Including the Flow Effect

Jean-Michel Ville
The George Washington University
Joint Institute for Advancement of Flight Sciences
Langley Research Center
Hampton, Virginia

Richard J. Silcox
Langley Research Center
Hampton, Virginia

National Aeronautics
and Space Administration

**Scientific and Technical
Information Branch**

1980

SUMMARY

An experimental study of the radiation of sound from an inlet as a function of flow velocity, frequency, duct mode structure, and inlet geometry has been conducted by using a spinning mode synthesizer to insure a given space-time structure inside the duct. Measurements of the radiation pattern (amplitude and phase) and of the pressure reflection coefficient have been obtained over an azimuthal wave number range of 0 to 6 and a frequency range up to 5000 Hz for two different inlets, an unflanged duct and a bellmouth.

The results of the investigation of the radiated field without flow and of the pressure reflection coefficient for the unflanged duct have been found to be mostly in good agreement with theory. A comparison between the unflanged duct and bellmouth measurements, in the case of no flow, has shown the effect of the inlet geometry on the radiated field and on the pressure reflection coefficient. The influence of the inlet contour appeared to be very drastic near the cut-on frequency of a mode. A reasonable agreement has been found between the measured pressure reflection coefficient for the bellmouth and a theoretical prediction made for a duct terminating with a hyperboloidal inlet extending to infinity.

The study of the influence of flow has been conducted by using the bellmouth for two mean-flow Mach numbers, 0.2 and 0.4. This investigation has shown that the flow has a very weak effect on the amplitude of the directivity factor and significantly shifts the phase of the directivity factor. A comparison between these experimental results and some existing theoretical predictions has shown poor agreement. However, the influence of the flow on the modulus of the pressure reflection coefficient has been found to be well described by a theoretical prediction.

INTRODUCTION

The noise radiated from the inlets of aircraft engines has become an increasingly important acoustic problem with the progress made in reducing jet noise. Various techniques to alleviate this noise problem, after its generation, have included the development of acoustic liners, high Mach number inlets, and the use of inlet geometry to redirect the sound. This study is directed towards experimentally investigating the influence of the inlet geometry by comparing two simple inlet shapes, an unflanged duct and a bellmouth. No previous theoretical or experimental investigations have studied this effect of the contour of a finite length inlet on the radiated field as a function of modal structure and mean Mach number. Therefore the purpose of this work is to demonstrate the geometry-induced effects on the reflected and radiated acoustic fields of these inlet shapes. The effect of various mean flows into the bellmouth inlet on the acoustic field is shown. In addition, a short description of the theory of operation and simple acoustic fields of the spinning mode synthesizer (SMS) incorporated into the flow duct facility are included.

In 1970 Lansing and others (ref. 1) proposed an exact solution to the problem of the radiation from an unflanged duct immersed in a uniform flow. Candel (ref. 2) and Homicz and Lordi (ref. 3) have shown how to calculate the radiated field from a duct immersed in a uniform flow if the no-flow solution is known. These studies have shown that, in the case of flow everywhere, the radiation pattern was not changed significantly for isolated propagating modes.

Two theoretical investigations have tried to compute or describe the effect of an internal flow on the radiation pattern, a condition required to model static tests. In 1975 Savkar (ref. 4) included the effect of mismatch between the flow inside the duct and no flow outside by using a model with two uniform flow regions. The first one is a plug flow region which includes the duct itself and its continuation outside, and the second region consists of the surrounding space. Although good agreement was found in reference 4 between his prediction and the experimental work made by Crigler and Copeland (ref. 5), this model appears to represent poorly a static test where the flow velocity in the acoustic far field is nearly zero. In 1979 Rice and others (ref. 6) developed a different theoretical approach to the same problem. They extended the relationship which exists in a no-flow situation, between the angle of incidence of the wave within the duct and the angle of the principal lobe of radiation, to the case with flow. This theoretical prediction has been compared with some experimental works by Heidmann and others (ref. 7). They concluded that the discrepancies found in the comparison were due to refraction effects at the face of the inlet. None of these theoretical works included the effect of the contour of the inlet, and the experimental measurements, taken with various contour inlets, are compared with these predictions because they are available.

Two investigations, one experimental and one theoretical, have included the effect of inlet geometry. In 1977 Sloan and others (ref. 8) conducted an experimental study of the effect of different inlets which provide different flow conditions inside the duct. One of these inlets was designed such that the effect of flow gradients had a small influence on the radiated field. Another was designed to refract strongly the acoustic wave away from the center line of the duct. The last one was an asymmetric combination intended to redirect the sound. These authors found a weak change of the radiation pattern when they increased the mean throat Mach number from 0.4 to 0.8 for the three inlets. They then conducted no-flow measurements by using an acoustic source which provided nearly the same wave structure inside the duct. By comparing the flow and no-flow measurements, they concluded that the effect of inlet geometry is much more important than the effect of the flow on the radiated field. In 1979 Cho (ref. 9) found the exact solution to the problem of radiation from hyperboloidal inlets. In the theoretical study of reference 9, which does not include any flow effect, the walls of the inlets are assumed to be infinite.

A spinning mode synthesizer, which provides a known wave structure inside the duct with and without flow, is used to investigate the radiated field as a function of frequency, azimuthal wave number, and mean-flow Mach number. Two such facilities are known to be in operation. One, which has been built by the University of Compiegne and Office National d'Etudes et de Recherches Aérospatiales (O.N.E.R.A.) (ref. 10), allows the choice of the radial as well as azimuthal wave number. This spinning mode synthesizer has been used recently to

verify the convection effect of the flow on the axial wavelengths (ref. 11) and also to measure the influence of the angle of incidence of the wave on the impedance of an absorbent material (ref. 12). The other one, which has been used during the experimental works presented, is described in the following part of this paper.

The experimental procedure and methods used to study the field radiated from an inlet are described first. Descriptions of the spinning mode synthesizer, flow duct facility, and various acquisiton procedures are included. The experimental results presented next include the radiation pattern, amplitude and phase, and the pressure reflection coefficient. First the measurements for the unflanged duct are compared with the theoretical computation without flow from reference 4. Then the study of the radiation from a bellmouth is presented. The experimental results are compared with those of the unflanged duct and reference 9. Finally the influence of the flow on the radiated field is shown by comparing the no-flow measurements and the results obtained for two flow conditions (mean Mach number equal to 0.2 and 0.4) using the bellmouth.

SYMBOLS

a	radius of duct, m
A_m	spinning mode pressure coefficient
c	speed of sound, m/sec
f	frequency, Hz
f_{mn}	cutoff frequency of mode, $\frac{c}{2\pi a} \chi_{mn} \sqrt{1 - M^2}$, Hz
k	total wave number, ω/c, m^{-1}
k_x^+	axial wave number of incident or upstream wave, m^{-1}
k_x^-	axial wave number of reflected or downstream wave, m^{-1}
(m,n)	azimuthal and radial wave numbers, respectively; (0,0) is plane wave
M	mean-flow Mach number
p	complex acoustic pressure, N/m^2
R	complex pressure reflection coefficient
S	minimization parameter
SPL	amplitude of directivity pattern, dB
t	time, sec

x	axial cylindrical coordinate
ΔPWL	difference in acoustic radiated power between bellmouth and unflanged inlet, dB (ref 10 pW)
$\Delta\phi_n$	phase difference between reference wall microphone and other microphones, deg
θ	azimuthal cylindrical coordinate
ϕ	phase of acoustic pressure with reference to phase of oscillator, deg
χ_{mn}	(n + 1)th zero of derivative of Bessel function of first kind and order m
ψ	polar spherical coordinate
ω	angular frequency, $2\pi f$

Abbreviation:

SMS	spinning mode synthesizer

APPARATUS AND PROCEDURE

Spinning Mode Synthesizer

The spinning mode synthesizer (SMS) is incorporated into the flow duct facility of the Langley Aircraft Noise Reduction Laboratory. The purpose of the SMS is to provide a turbomachinery-type noise source for the experimental investigation of the propagation of noise in finite length ducts and of the radiation from the duct to the environment in a tightly controlled laboratory situation.

Spinning mode generation.- The spinning mode synthesizer incorporated into the flow duct facility is a research apparatus designed to overcome the problems involved in static testing of real turbofan engines or research fans. The SMS generates arbitrary combinations of acoustic sound patterns at a specified frequency in the presence of airflow in a 0.3-meter duct. Specified duct modes are generated by controlling the amplitude and phase of 24 acoustic drivers equispaced around the duct wall in a plane perpendicular to the duct center line. By properly adjusting the input to the drivers, individual spinning modes, a combination of modes, or circumferential standing waves may be generated in the duct. The acoustic field produced by the array of drivers is monitored by an array of 48 wall-mounted microphones located 0.2 meter upstream of the drivers. At these microphone locations the desired acoustic wall pressures (amplitude and phase) are approximated to some arbitrary degree of accuracy. In order to attain this accuracy, the pressure field sensed by the 48 microphones feeds back

through a control computer optimization algorithm to generate correction signals to the drivers. Thus, by an iterative process, the pressure field at the microphone array converges to some specified target pressure at the monitoring array. Once the target pressure is attained, the mode setup may be stored by recording the driver settings for future recall or the steady-state acoustic field may be left intact for experimental studies.

Optimization method.- The optimization algorithm referred to in the previous section is a model of a second-order differential equation having 48 degrees of freedom. The degrees of freedom are the amplitude and phase control exerted over each of the 24 acoustic drivers. Thus the effect of each degree of freedom must be taken into account in moving from one system state to another.

The progress towards attaining the desired system state (desired acoustic field at the monitoring microphones) is measured by the "system error." This error is defined as the sum of the squared differences between the desired complex pressure and the measured complex pressure at each monitoring microphone. Using the system error as the optimization parameter, the algorithm consists of two parts.

The first step consists of defining an optimum direction in 48 dimensional space to move the driver amplitudes so as to minimize the system error most effectively. This step is accomplished by applying a small increment to the real and then imaginary part of the input of each acoustic driver. The effect is then noted on the system error and the change in system error is then stored as one component of a 48 dimensional vector. This routine is done for each component of each driver, and the resultant vector defines the optimum direction along which to move the excitation to achieve the desired response.

Having defined this direction vector, the second part of the optimization algorithm consists of determining the optimum step along the course of the direction vector that minimizes the system error. Since the system behaves ideally as a second-order equation, the step is optimized as a series of parabolic approximations. Using the current system state as a starting point, two additional steps along the previously determined direction are taken, noting the new system error each time. Plotting the step size as the abscissa and the system error as the ordinate, the system fits a parabola through the three points and computes the point of minimum error and the curvature. If a good fit is not established, the step size is varied until three points are found that provide a good fit. In this way the system error function is minimized.

If the system error is within the allowable error of the target acoustic field, the optimization routine exits and the mode is set up. However, if the system error is not within an acceptable error, the process repeats. A new direction vector is established from the current system state and the process continues to convergence.

Wave number verification.- The complex pressures recorded at the 48 wall-mounted microphones of the SMS are decomposed into an azimuthal wave number

spectrum at the end of the optimization process. This decomposition is a Fourier type of expansion of the spatial pressure distribution into

$$p(\theta) = \sum_{m=-N}^{N} A_m e^{im\theta} \tag{1}$$

which yields a sound pressure measurement for each spinning mode order (including the plane wave) up to a maximum of 24. The information is available immediately upon completion of the optimization process and on request thereafter. Therefore the time stability of the acoustic field may also be checked.

In addition to the calculation of the azimuthal wave number spectrum, a check on the axial wave number is made. By assuming that only the desired mode is propagating, the theoretical axial wavelength over the axial microphone array is calculated and compared with the measured axial wavelength.

Figures 1 and 2 show the azimuthal wave number content and the comparison of the theoretical and measured phase for a spinning order of 1, first radial mode (1,0) at a frequency parameter of 3.76 for two different inlets and Mach numbers. The spectra show the level of this mode to be more than 19 dB without flow and 13 dB with flow above other extraneous modes in the duct. The agreement of the phase variation in each case shows that the desired mode dominates the acoustic field.

Pressure Reflection Coefficient

The method used to compute the pressure reflection coefficient is an extension to that used by references 13, 14, and 15 for the plane wave situation.

The method used is a least-squares fit to the complex acoustic pressure measured at nine different axial wall locations inside the duct at the same azimuthal position. The principal assumptions are that only one mode is incident in the duct, that only the same mode is reflected by the open end of the duct, and that the flow is uniform. The acoustic pressure inside the duct is characterized by an incident and reflected wave (fig. 3) of the form

$$p_i = p_{i} e^{i(k_x^{+} x - \omega t)} \tag{2a}$$

$$p_r = p_{r} e^{i(k_x^{-} x - \omega t)} \tag{2b}$$

where p_i is the incident wave, and p_r is the reflected wave. By solving nine complex equations in two complex unknowns in a least-squares sense, the residual that is minimized is given by

$$S = \sum_{j=1}^{9} \left\{ [p(x_j) - p_i(x_j) - p_r(x_j)] [p(x_j) - p_i(x_j) - p_r(x_j)]^* \right\} \qquad (3)$$

where $p(x_j)$ is the complex pressure measured at point x_j and * indicates a complex conjugate. The residual is minimized with respect to the real and imaginary parts of the incident and reflected pressure coefficients. This minimization results in a complex pressure reflection coefficient which is then corrected in phase to a reference plane at the beginning of the constant area section of the inlet. This location corresponds to the end of the unflanged duct and the downstream end of the bellmouth inlet section.

This analysis technique has been compared with the two-microphone method used in reference 16 and shown to be in very good agreement for spinning modes of all orders. In addition, this technique avoids the problem noted by Johnston and others (ref. 15) of microphone spacing in the two-microphone method. For microphone spacings approaching multiples of one-half the axial wavelength, the two-microphone method provides erroneous results. However, as long as the nine microphones are randomly spaced axially on the duct, the least-squares technique provides more reliable results.

Experimental Facilities

Flow anechoic chamber.- The inlet duct test apparatus is mounted in the flow duct facility of the Langley Aircraft Noise Reduction Laboratory and extends into the anechoic chamber shown by the plan view in figure 4. This anechoic chamber measures 9.15 meters wide by 6.1 meters deep by 7.16 meters high. The flow facility is essentially an open-circuit wind tunnel. The flow circulation in the facility is provided by a centrifugal blower which pulls air through a 0.3-meter-diameter flow duct using the anechoic chamber as a plenum. Air is supplied to the anechoic chamber through a large supply duct on the rear wall. A photograph of the bellmouth inlet mounted in the anechoic chamber is shown in figure 5. This flow facility is operable over an inlet Mach number range of 0 to 0.5.

Flow spinning mode synthesizer.- This device consists of 24 acoustic drivers equispaced circumferentially at one axial location (fig. 6). The variation of the amplitude and phase of the signal to each acoustic driver is achieved by multiplying orthogonal sinusoidal outputs from the master oscillator by digital gains and adding the results together to form an oscillatory signal of specific amplitude and phase relative to the oscillator (fig. 7). In this way, each driver can be set over a wide range of amplitudes with arbitrary phase and remains in this same state until specifically altered by the computer.

Test inlets.- Two different duct configurations were used for these tests. The unflanged duct shown in figure 8 and the bellmouth inlet used a common configuration up to where the nine microphones are mounted. Here the 0.46-meter unflanged duct is replaced with a 0.3-meter hardwall section and the bellmouth inlet (fig. 5). For the investigation of the radiation from the bellmouth, aerodynamic instrumentation is installed upstream of the wall microphone sections. Some additional sections in both cases are used to provide the same overall length, 4.35 meters, for both configurations between the acoustic drivers and the face of the inlet. Photographs of the two inlets are shown in figures 9 and 10(a). A side-cut view of the bellmouth is given in figure 10(b).

Instrumentation and Data Reduction

Acoustic measurements.- Nine 6.35-mm-diameter condenser microphones are flush mounted on the wall of two sections to provide the measurement of the pressure reflection coefficient and the verification of the proper axial phase variations of the wave structure.

The measurement of far-field pressure is provided by a 1.27-cm-diameter condenser microphone mounted on a traversing boom. This microphone is traversed in a horizontal arc at a 3.05-meter radius from the center point at the face of the inlet in both cases (unflanged duct and bellmouth) (fig. 4). A motor allows a slow and constant speed displacement of the transducer.

The acoustic data acquisition system is illustrated in block-diagram form in figure 11. All of the microphone data, the source section microphones and the test section microphones are analyzed by the same method. The 48 source section microphones are ceramic transducers. With the associated electronic conditioning, these microphones have a range of 70 to 135 dB, and stored calibration information corrects for variations in sensitivity with frequency. The other measurement microphone signals are conditioned and multiplexed together and the analog signal is fed into the SMS multiplexer board along with the source section microphone outputs. From here, all microphone signals are treated in common. A programmable gain amplifier provides a signal suitable for digitizing, and a tracking filter provides 100-Hz bandwidth filtering centered on the oscillator frequency. This is the same oscillator used to provide the primary drive to the acoustic drivers so that all filtering operations are based on this master oscillator. This operation eliminates most of the flow noise and provides a high level, stable signal to be digitized.

The digitizing process is performed using a 12-bit analog-to-digital system utilizing a trigger feature to initialize data acquisition always at the same point on the rising side of the master oscillator input to the trigger. The purpose of this technique is twofold. First, a signal enhancement technique can be employed to filter the uncorrelated noise within the passband and to average amplitude and phase variations. Secondly, this provides a true reference phase common to all microphone measurements by which they may be compared.

The final signal enhanced data of 160 data points over 10 or more cycles of the oscillator signal is fit in a least-squares sense to a sine wave of the driving frequency and arbitrary amplitude and phase. This curve fitting is an

additional filtering process of extremely narrow passband and provides a reliable final measurement of the amplitude and phase.

The far-field microphone data are analyzed in exactly the same manner. However, since the boom is swept continuously, some spatial averaging is also involved. A computer-initiated command starts the far-field boom to sweep from -95° to 95° in arc position. Position feedback information initiates an acquisition sequence from the microphone typically every degree of arc rotation. Therefore each data point plotted is an average over approximately 1 second of time and 1 degree of rotation. A block diagram of the boom control is shown in figure 12.

Aerodynamic measurement.- The mean-flow Mach number is measured by using four static pressure taps spaced 90° circumferentially at the same axial location 1.02 meters downstream of the inlet face. These taps are connected to one pressure transducer. The taps are scanned mechanically using a 0 to 51.7 kN/m^2 transducer. This signal is conditioned and then digitized directly. The four pressures are averaged, and by using the current barometric pressure, the mean-flow Mach number is calculated using standard compressible flow relations.

RESULTS AND DISCUSSION

The test conditions of this experimental study are presented for various azimuthal wave numbers and frequencies (table I). Each acoustic pressure field had been previously set up by using a foam wedge duct termination to simulate an infinite length duct. Each mode setup is characterized by specified driver inputs representing driver amplitudes and phases, which are stored in the computer. The excitation of the drivers remains constant whatever the duct termination and flow situation. This method assumes that the effects of the reflection and flow on the impedance of the drivers are negligible.

Sound Radiation From an Unflanged Duct Without Flow

The far-field directivity and complex reflection coefficients reported in this section are compared with Savkar's theory (ref. 4). His study without flow predicts the amplitude and phase of the radiated field and the complex reflection coefficient from an unflanged circular duct.

Pressure reflection coefficient.- The pressure reflection coefficient is analyzed from an axial array of nine microphones by using the method described previously. Data are presented for all the cases shown in table I where only a single radial mode is cut on.

Figure 13(a) shows a comparison of measured and theoretical (ref. 4) reflection coefficient moduli for modes (0,0), (1,0), (2,0), (4,0), and (6,0). The comparison is very good in the plane wave case for higher values of reflection coefficient. However in this case and also for the higher order modes, as the modulus of the reflection coefficient decreases, the magnitude of the reflected wave approaches that of extraneous modes in the duct. This violates

an assumption of the analysis and reduces the confidence in both the amplitude and phase data at values of $|R|$ less than about 0.1, depending upon the isolation of the desired mode. The theory for the higher order modes underpredicts the measurement by 0.2 or more near the cut-on frequency of the mode. However the trend is the same with the theory and measurement converging at higher values of ka above cut-on.

The comparison of the phase of the pressure reflection coefficient is shown in figure 13(b). The data again show the same trend as the theory; however the measured values have a steeper slope near the mode cut-on frequencies, and the peak values are more than 150° higher than those predicted by Savkar.

Radiated field.- Some representative comparisons of measured and theoretical far-field radiation directivities are shown in figures 14(a) to 14(f). These curves are presented in terms of a directivity index, relative to the maximum against polar angle over a 40-dB range. Figure 14(a) shows the measured and predicted directivity of the radiated field for the plane wave with a frequency parameter of 3.76. The agreement is within 0.5 dB from -50° to 50° polar radiation angle.

The remaining data presented are for spinning modes. In figure 14(b) are plotted the measured and predicted directivity of the radiated field against polar angle for mode (1,0) at a frequency parameter of 2.03. The frequency ratio, defined as the ratio between the exciting frequency and the cutoff frequency of a mode, is 1.11. The discrepancy is only 2.5 dB over a range of 30° centered about the principal radiation angle of mode (1,0). However the poor comparison around the center line can be explained as follows. The spinning mode synthesizer has set up a mode (1,0) with a level 20 dB higher than the level of the plane wave in the duct, but the reflection coefficient of the mode (1,0) is much higher than the reflection coefficient of the plane wave at the same frequency. This reflection of energy of mode (1,0) makes the plane wave radiate from the duct with a level close to that of the first spinning mode. At a frequency parameter of 5.29, the mode (1,0) has a much lower reflection coefficient and the agreement between the predicted and measured values is better than 1 dB except for right on the center line (fig. 14(c)).

Representative examples for the mode (2,0) at two different frequency ratios, 1.11 and 1.74, are presented in figures 14(d) and 14(e). The same trend as for the previous examples can be observed. Finally the measured and predicted directivity patterns are compared in figure 14(f) for a higher mode (6,0) at a frequency ratio of 1.49. The agreement is within 2 dB throughout the region dominated by the principal lobe of the mode (6,0). The plane wave again is dominating the radiation at the center line.

Two examples of the variation of the phase plotted against the polar angle are presented. The first one (fig. 15(a)), for the plane wave at a frequency parameter of 1.39, shows good agreement between experiment and theory except near the center line. This phase variation is typical for an even mode. The second example (fig. 15(b)) concerns the phase variation of the mode (1,0) and a frequency parameter of 2.66 as a function of the polar angle. The agreement is also good. The phase shift which separates these two curves is due to different phase references.

Sound Radiation From a Bellmouth Without Flow

The results of the experimental investigation of the reflected field from a bellmouth inlet (fig. 10) are compared with the experimental data of the unflanged duct and also with the pressure reflection coefficients predicted for a 57° hyperboloidal inlet (ref. 9). Also a comparison of the radiated field is made with that of the unflanged duct to show the influence of the inlet geometry on the directivity pattern.

Pressure reflection coefficient.- Figure 16(a) shows the variation of the modulus of the pressure reflection coefficient for the unflanged duct, for the bellmouth inlet, and from reference 9. Data are shown for modes (0,0), (1,0), (2,0), (4,0), and (6,0). A comparison of the experimental data shows a marked reduction of the pressure reflection coefficient of the bellmouth over the unflanged duct. Near the cut-on frequency of each mode this difference varies from 0.25 to 0.4, but converges in each case as ka increases. Thus the influence of geometry of an inlet is more important near the cut-on frequency of a mode. A comparison of Cho's theory (ref. 9) with the bellmouth data shows a reasonable agreement even near cut-on, where the theory overpredicts by about 0.15. This difference again decreases as the frequency parameter is increased.

The phase of the reflection coefficient is presented in figure 16(b) and shows the same comparisons as the previous figure. The phase delay of the bellmouth increases over that of the unflanged duct, for all modes considered, but the trend for both inlets is the same. The comparison of the theory (ref. 9) shows reasonable agreement over the range of coefficients that could be measured, both in trend and absolute values. The increased discrepancy noted for the modulus near the mode cut-on frequencies does not appear in the comparison of phase.

Radiated field.- Figure 17(a) shows the variation of the sound pressure level directivity of the radiated field with the polar angle for both inlet configurations. The plane wave has been set up with a frequency parameter of 1.39. The level starting at an absolute value of the angle of 45° is higher for the unflanged duct than for the bellmouth. Standing waves due to the anechoic chamber facility induce the fluctuation noted. Figure 17(b) presents a plane wave with a frequency parameter of 3.76. The two curves closely match with the unflanged duct again radiating higher levels to the sidelines.

Figures 17(c) and 17(d) show the effect of inlet geometry on the radiation of spinning modes. Figure 17(c) compares the inlets for a mode (1,0) and a frequency ratio of 1.44; figure 17(d), the same mode at a frequency ratio of 2.87. The shift of the angular location of the principal lobe of radiation is almost 20° for the lower frequency case, the bellmouth tending to move this location closer to the center line of the duct.

In order to show the effect of inlet geometry on the radiated field more clearly, the concept of the angular location of the predominant acoustic radiation is introduced. This representation is illustrated in figure 18. An example of the variation of the sound pressure level against the polar angle is plotted. If the maximums of the curve are associated with two values of the

angle, one on each side of the center line of the duct ($\psi = 0$), four angles characterize the value of the amplitude equal to the maximums minus 6 dB. These angles starting from -95° to 95° are ψ^-_{min}, ψ^-_{max}, ψ^+_{min}, and ψ^+_{max}. From an experimental measurement of the radiation pattern, for a given mode and frequency, these four values of the angle are derived. The variation of these angles with the frequency ratio is shown in figures 19(a), 19(b), and 19(c) for modes (1,0), (3,0), and (6,0), respectively. These curves describe not only the variation of the width of a lobe $(\psi^-_{max} - \psi^-_{min}, \psi^+_{max} - \psi^+_{min})$ on both sides of the center line of the duct but also the change of the location of the principal radiation for one mode when the frequency ratio is increased. As can be seen on these curves, the width of the principal lobe of radiation is strongly modified by the contour of the bellmouth compared with the unflanged duct. The largest discrepancy occurs near the cut-on frequency of a mode at the outer angles $\psi^\pm_{max}$ where the difference reaches 15° to 20°. Near the center line both curves are similar. As the frequency ratio increases, the two curves converge for the three modes concerned. The frequency ratio where this convergence occurs depends upon the azimuthal wave number. The three values of this ratio are 3, 2, and 1.5 for modes (1,0), (3,0), and (6,0), respectively. These curves also show for both configurations that the width of the principal lobe of radiation decreases as the frequency increases.

Figures 20(a) and 20(b) present the directivity of the radiated field from the bellmouth at different frequency parameters for modes (1,0) and (2.0), respectively. These figures demonstrate the location of the principal lobe of radiation shifts closer to the center line of the duct when the frequency (and f/f_{mn}) is increased.

Figure 21(a) shows the variation of the phase of the directivity pattern with the radiation angle for both inlet configurations for a plane wave with a frequency parameter of 1.39. The phase reference is the same in both cases. The shift observed can be explained by the fact that the phase of the mode is modified by the acoustic termination at the end of the duct which is different for each case at such a low frequency. Note that the trend of the phase remains similar around the center line up to an angle of 35° where a large difference occurs and increases with the angle from the center line. Figure 21(b) shows the inlet geometry effect on the phase variation for an odd mode (1,0) at a frequency parameter of 2.66. The trend of the curve again is modified strongly at angles greater than 35°.

A shielding effect cannot be used to explain either this effect or that noted on the amplitude directivity since the pivot of the boom is centered under the highlight of both inlets. The prediction of the amplitude directivity may be possible if the change in duct radius, which occurs along the length of the bellmouth, is taken into account. The value of the appropriate radius depends upon the space-time structure of the wave, but the variation of the far-field phase cannot be explained with this effect.

The data curves displayed in figure 22 represent the variation of the difference of the radiated power between the two configurations as a function of

the frequency parameter and the azimuthal wave number. The most important difference occurs near the cut-on frequency of a mode where the bellmouth radiates much more acoustic power than the unflanged duct.

Influence of Flow on Radiation From a Bellmouth

The experimental results of the study of the radiated field from a bellmouth (fig. 10) are presented for an internal flow situation. The range of frequencies and azimuthal wave numbers is given in table I. The no-flow results are compared with the results for mean-flow Mach numbers of 0.2 and 0.4 to point out the effect of the flow on the induct and radiated acoustic fields. The effect on the pressure reflection coefficient is also compared with an expression developed in reference 17.

Pressure reflection coefficient.- The effect of an inlet Mach number of 0.2 on the modulus of the pressure reflection coefficient for modes (1,0), (2,0), and (4,0) is shown in figure 23(a). The magnitudes of the reflection coefficients are reduced 0.1 to 0.3 near the cut-on frequencies of each mode by this flow. Again the effect diminishes as ka is increased above those values at cut-on. The lines of this figure connect the no-flow measurements corrected by the factor $\left(\frac{1 - M}{1 + M}\right)^{1.33}$ of reference 17. This factor corrects the no-flow data to within 0.1 of the flow data near the cut-on frequencies, and the correlation improves as ka is increased. The reflection coefficient data for higher flow rates become more uncertain because of the continual decrease in magnitude of the reflected wave, thus violating the assumptions of the analysis. Thus the data are not shown for a Mach number of 0.4 or for the higher mode numbers for which there exists an increased number of extraneous modes to mask the one of interest.

Figure 23(b) shows the effect of the flow at a Mach number of 0.2 on the phase of the reflection coefficient. A shift or phase delay of 50° to 90° is observed to be introduced near the cut-on frequency of each mode, although for the mode (1,0) the flow and no-flow values converge as ka is increased. This convergence is not the case for the mode (2,0), where an 80° shift is evident throughout the range of ka plotted.

Radiated field.- In figure 24(a) is displayed the variation of the sound pressure directivity with the polar angle for the plane wave with a frequency parameter of 1.39. The curves show the no-flow case and 0.2 and 0.4 mean-flow Mach number cases with the maximums having been matched for comparison. The small-scale spatial variations noted for these cases are due to standing waves in the test facility. A 5-dB discrepancy occurs between the no-flow curve and the flow curves for angles greater than about 40°. The two flow curves are identical. Changing the Mach number from 0.2 to 0.4 does not modify the radiation pattern.

Figures 24(b) and 24(c) show a comparison between no-flow and 0.4 mean-flow Mach number measurements of the directivity of the radiated field for the same azimuthal wave number (2,0) and the frequency parameters of 3.37 and 4.4. The

same comparison between no-flow and flow measurements is presented in figure 24(d) for a higher mode (4,0) and a frequency parameter of 5.81. The curves indicate that the flow does not modify the shape of the radiation pattern and, consequently, the location of the maximum of the radiation, whatever the frequency ratio is. Note that in figure 24(d) the small-scale spatial variations that dominate all these spinning mode plots are due to small velocity fluctuations inducing variations in the structure of the acoustic field rather than the standing waves noted at a low frequency.

Two typical examples which demonstrate the effect of flow on the phase of the radiated acoustic field are shown in figures 25(a) and 25(b). The first example (fig. 25(a)) shows the variation of the phase for a plane wave at a frequency parameter of 1.39. The three curves are for the no-flow and two mean-flow cases. The effect of the flow will certainly account for a uniform shift of the far-field phase; however, the flow also flattens out the phase at the higher angles to that which was shown to be typical of the unflanged duct. The phase measurements presented allow for maximum phase differences of 360°; thus the phase for the 0.4 mean-flow Mach number case is really shifted through more than 1 cycle. The second example (fig. 25(b)) shows an odd mode (1,0) at a frequency parameter of 2.03. The same phenomenon is observed for this case; that is, the flow flattens the phase variation at higher angles and makes it resemble the phase variation of an odd mode radiated from an unflanged duct.

Reference 8 predicts that the effect of the flow is to make the location of the principal lobe of radiation closer to the center line of the duct. This effect is associated with the decrease of the axial wavelength of the upstream traveling wave. The comparison between the no-flow and flow measurements presented in this section indicates a poor agreement with this prediction. The examples presented for modes (2,0) and (4,0) with a no-flow frequency ratio of 1.11 show that the location of the principal lobe of radiation is not modified by the flow. According to the theoretical prediction, this angle should shift 25° toward the center line for a Mach number of 0.4. Even if reflection effects off the inlet are considered, a noticeable shift should be detectable. The effect of the flow on the far-field radiated phase also indicates that the flow effect is different from the frequency effect to which reference 8 ascribes it.

CONCLUDING REMARKS

Experimental results and theory for the directivity pattern of an unflanged duct with no flow have been found to be in good agreement. A comparison between the prediction of the reflection coefficient and the experimental measurements indicates that the theory underpredicts the value of this pressure reflection coefficient. The discrepancy is greater near the cut-on frequency of a mode.

A comparison of arbitrary inlet shapes and unflanged or flanged duct theories is not possible near the cut-on frequency of a mode. The frequency ratio where this comparison becomes reasonable depends upon the space-time structure of the wave and the contour of the inlet. The no-flow measurements

with this bellmouth indicate the significant effects of inlet geometry on the radiation pattern and on the pressure reflection coefficient near the cut-on frequency of a mode. The unflanged duct and the bellmouth radiation patterns tend to converge as the frequency ratio is increased. A comparison between the pressure reflection coefficients measured and theoretically predicted for a 57° hyperboloidal inlet shows good agreement with the bellmouth inlet data.

The effect of a uniform flow on the radiation pattern under static test conditions has been found to be unsatisfactorily described by existing theory. The study of the effect of a uniform flow on the sound radiated from the bellmouth shows that, for single propagating modes, the variation of the amplitude of the radiation pattern with the polar angle is not modified. The phase of the radiation pattern is shifted as the Mach number is increased.

The effect of a uniform flow on the pressure reflection coefficient is well described by existing theoretical predictions. A comparison between no-flow and flow measurements for the same inlet shows that the pressure reflection coefficients decrease as the Mach number increases.

Langley Research Center
National Aeronautics and Space Administration
Hampton, VA 23665
July 23, 1980

REFERENCES

1. Lansing, D. L.; Drischler, J. A.; and Pusey, C. G.: Radiation of Sound From an Unflanged Circular Duct With Flow. NASA paper presented at the 79th Meeting of the Acoustical Society of America (Atlantic City, N.J.), Apr. 21-24, 1970.

2. Candel, S. M.: Acoustic Radiation From the End of a Two-Dimensional Duct, Effects of Uniform Flow and Duct Lining. J. Sound & Vib., vol. 28, no. 1, May 8, 1973, pp. 1-13.

3. Homicz, G. F.; and Lordi, J. A.: A Note on the Radiative Directivity Patterns of Duct Acoustic Modes. J. Sound & Vib., vol. 41, no. 3, Aug. 8, 1975, pp. 283-290.

4. Savkar, S. D.: Radiation of Cylindrical Duct Acoustic Modes With Flow Mismatch. J. Sound & Vib., vol. 42, no. 3, Oct. 8, 1975, pp. 363-386.

5. Crigler, John L.; and Copeland, W. Latham: Noise Studies of Inlet-Guide-Vane-Rotor Interaction of a Single-Stage Axial-Flow Compressor. NASA TN D-2962, 1965.

6. Rice, Edward J.; Heidmann, Marcus F.; and Sofrin, Thomas G.: Modal Propagation Angles in a Cylindrical Duct With Flow and Their Relation to Sound Radiation. AIAA Paper 79-0183, Jan. 1979.

7. Heidmann, M. F.; Saule, A. V.; and McArdle, J. G.: Analysis of Radiation Patterns of Interaction Tones Generated by Inlet Rods in the JT15D Engine. AIAA Paper 79-0581, Mar. 1979.

8. Sloan, Denis; Farquhar, Bannister W.; and Rayl, Christopher: The Influence of the Inlet Duct Contour on Forward Radiated Fan Noise. AIAA Paper 77-1355, Oct. 1977.

9. Cho, Y. C.: Sound Radiation From Hyperboloidal Inlet Ducts. AIAA Paper 79-0677, Mar. 1979.

10. Ville, Jean-Michel: Definition and Realization of a Spinning Mode Simulator. ESA-TT-514, Sept. 1978.

11. Perulli, Mariano; and Ville, J. M.: Measurement of Absorbing Materials Acoustic Parameters in the Working Conditions of an Intake Duct. AIAA Paper 77-1332, Oct. 1977.

12. Perulli, M.; Lewy, S.; Lambourion, J.; and Ville, J. M.: Propagation Du Son Dans Un Conduit a Parois Absorbantes. Groupe Sectoriel Franco-Sovietique Industries Aeronautiques, Sous-Groupe A.A.A.S.: Aerodynamique, Acoustique, Aeronautique Et Structure (Moscow), May 21-28, 1979.

13. Schlinker, Robert H.: The Transmission of Acoustic Plane-Waves at a Jet Exhaust. AIAA Paper 77-22, Jan. 1977.

14. Seybert, A. F.; and Ross, D. F.: Experimental Determination of Acoustic Properties Using a Two-Microphone Random-Excitation Technique. J. Acoust. Soc. America, vol. 61, no. 5, May 1977, pp. 1362-1370.

15. Johnston, J. P.; and Schmidt, W. E.: Measurement of Acoustic Reflection From an Obstruction in a Pipe With Flow. J. Acoust. Soc. America, vol. 63, no. 5, May 1978, pp. 1455-1460.

16. Seybert, A. F.; and Parrott, T. L.: Impedance Measurement Using a Two-Microphone, Random-Excitation Method. NASA TM-78785, 1978.

17. Lumsdaine, E.: Calculation of Pressure Reflection Ratio. J. Sound & Vib., vol. 52, no. 1, May 8, 1977, pp. 145-147.

TABLE I.- LIST OF FREQUENCIES AND AZIMUTHAL WAVE NUMBER STUDIES

Frequency, f, Hz	Mode		Frequency parameter, ka	Frequency ratio, f/f_{mn}		
	m	n		M = 0	M = 0.2	M = 0.4
502	0	0	1.39	∞	∞	∞
1008	0	0	2.79	∞	∞	∞
1359	0	0	3.76	∞	----	----
689	1	0	1.91	1.02	1.03	1.07
734	1	0	2.03	1.10	1.12	1.20
815	1	0	2.25	1.22	1.25	1.33
960	1	0	2.66	1.44	1.47	1.57
1359	1	0	3.76	2.04	2.08	2.22
1912	1	0	5.29	2.87	----	----
1143	2	0	3.16	1.04	1.06	1.13
1218	2	0	3.37	1.11	1.13	1.21
1348	2	0	3.73	1.23	1.25	1.33
1359	2	0	3.76	1.24	1.26	1.35
1591	2	0	4.40	1.45	1.47	1.58
1912	2	0	5.29	1.74	1.77	1.89
1912	3	0	5.29	1.26	1.29	1.38
2516	3	0	6.96	1.66	1.69	1.81
2820	3	0	7.80	1.86	1.90	----
1990	4	0	5.51	1.04	1.06	1.13
2122	4	0	5.81	1.11	1.13	1.21
2346	4	0	6.49	1.22	1.25	1.33
2768	4	0	7.66	1.44	1.47	1.57
3322	4	0	9.19	1.73	----	----
2807	6	0	7.77	1.04	1.06	1.13
2994	6	0	8.28	1.11	1.13	1.21
3322	6	0	9.29	1.22	1.25	1.33
3907	6	0	10.81	1.44	1.47	1.57
4027	6	0	11.14	1.49	----	----

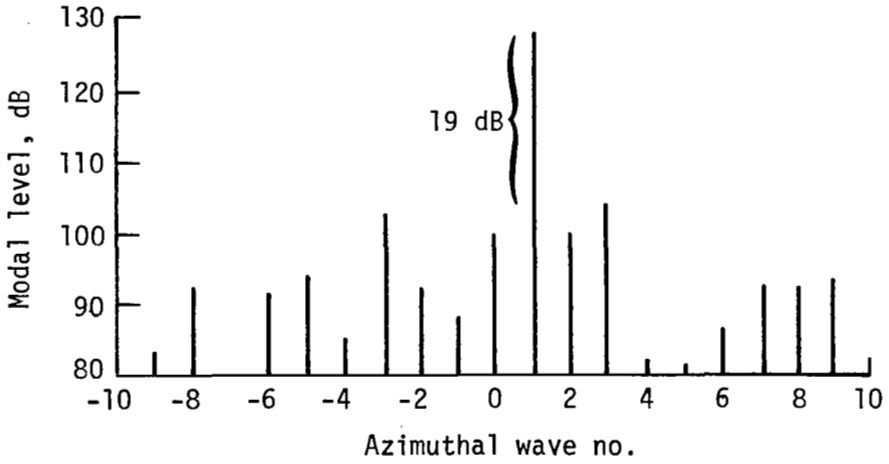

(a) Azimuthal wave number spectrum.

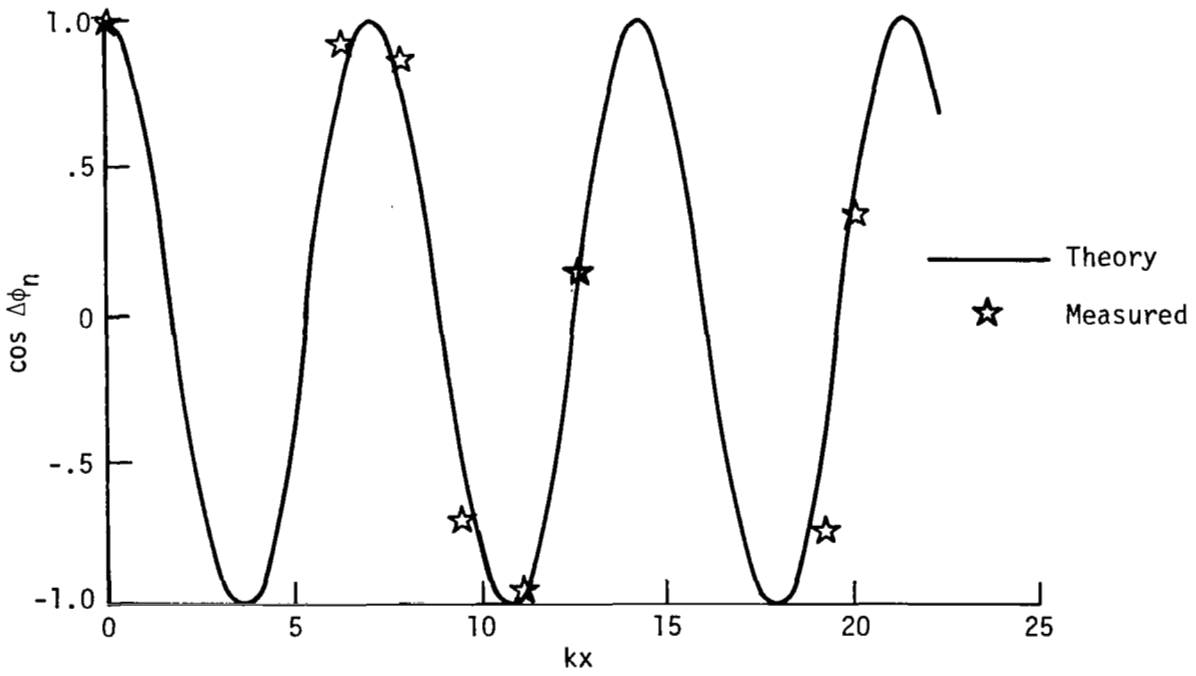

(b) Measured and theoretical axial wave structure.

Figure 1.- Source structure for (1,0) mode in unflanged duct with frequency parameter of 3.76 and M = 0.

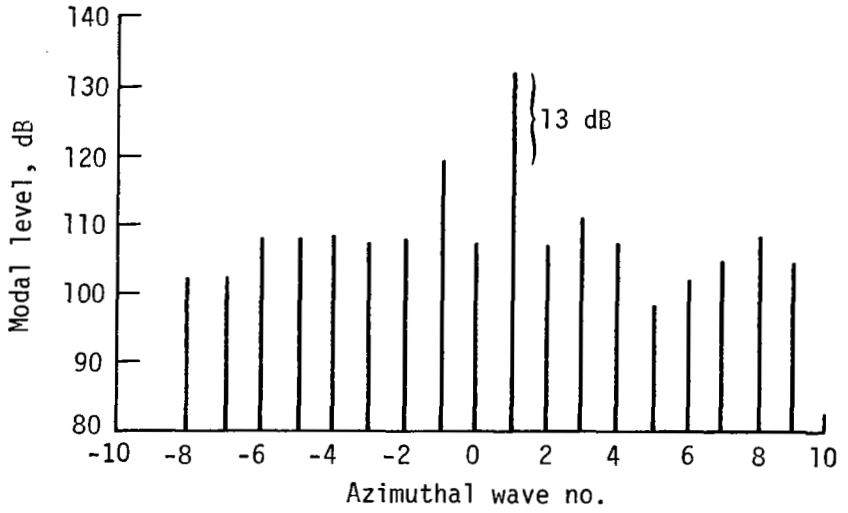

(a) Azimuthal wave number spectrum.

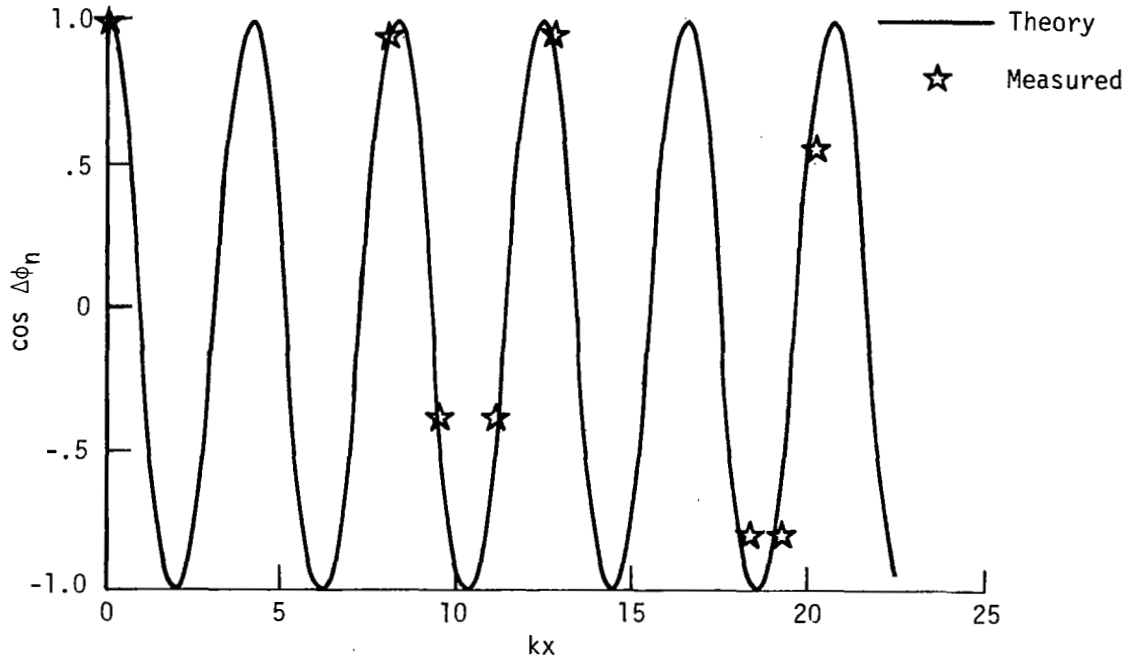

(b) Measured and theoretical axial wave structure.

Figure 2.- Source structure for (1,0) mode with bellmouth inlet, frequency parameter of 3.76, and M = 0.4.

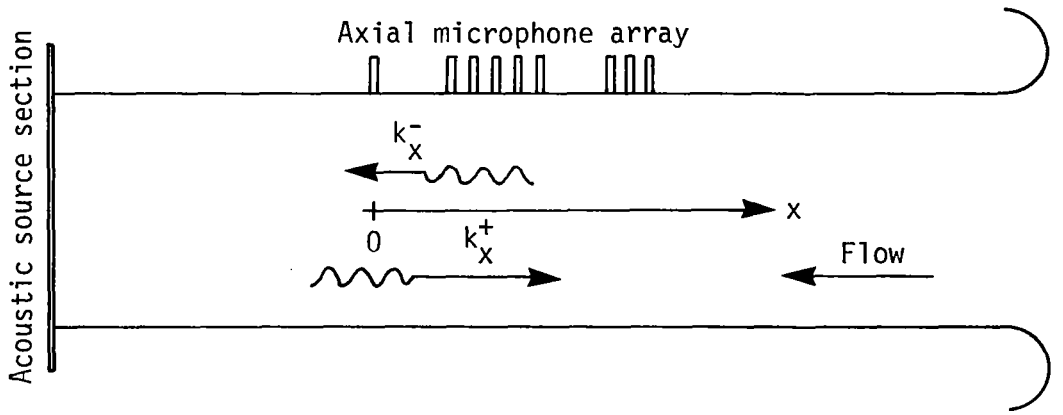

Figure 3.- Model of duct for acoustic pressure reflection coefficient theory.

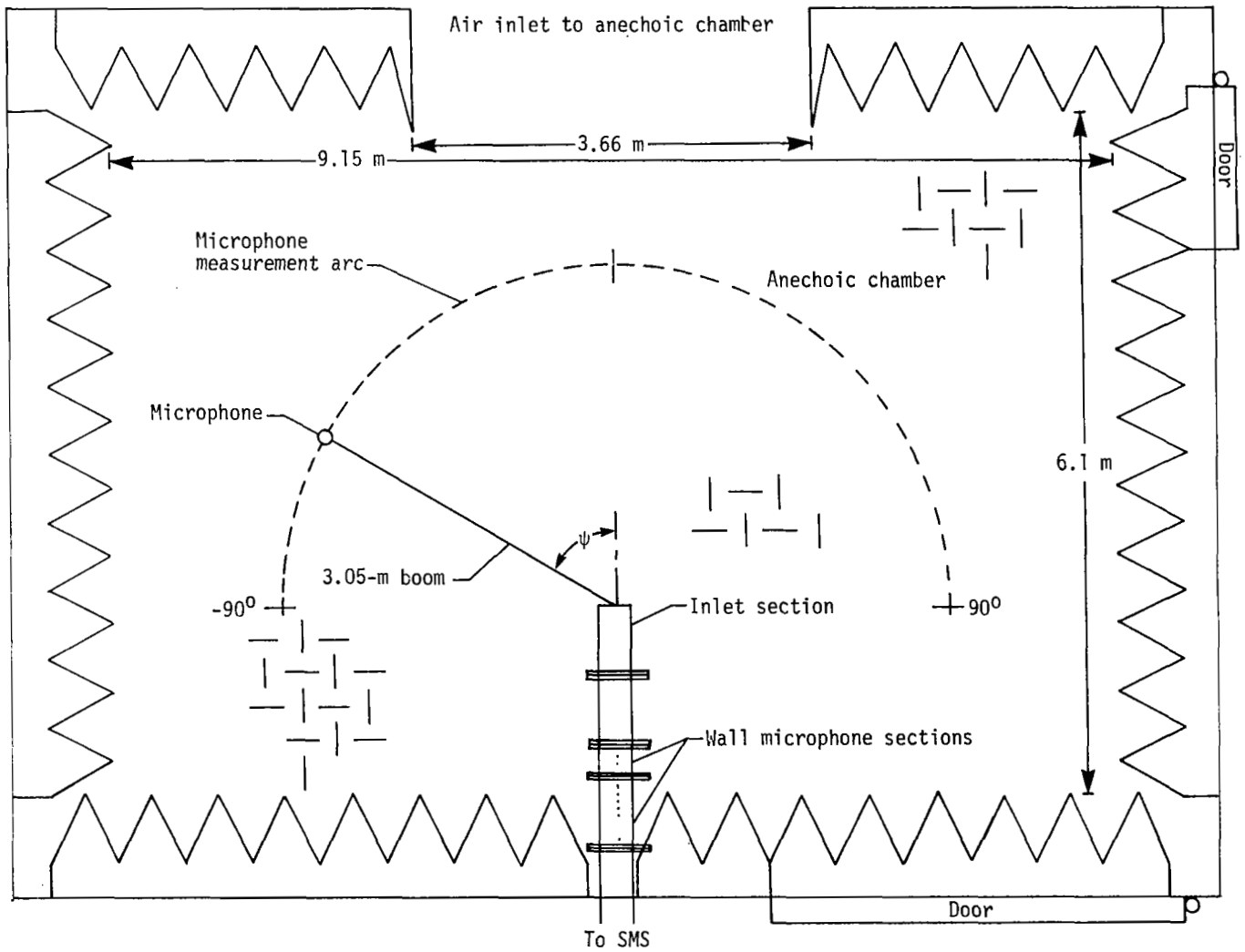

Figure 4.- Plan view of test facility.

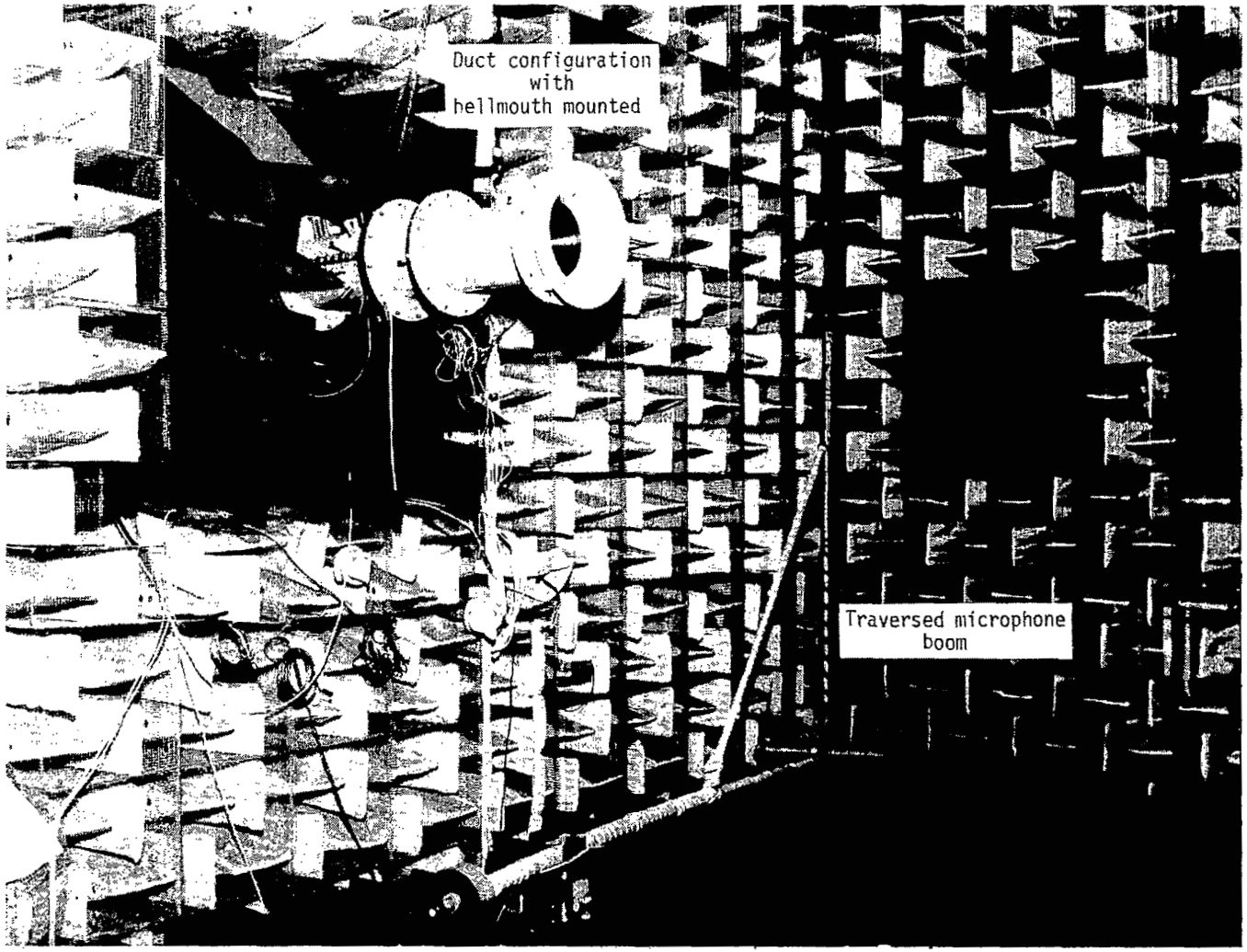

L-79-790

Figure 5.- Photograph of anechoic chamber flow duct facility of Langley Aircraft Noise Reduction Laboratory.

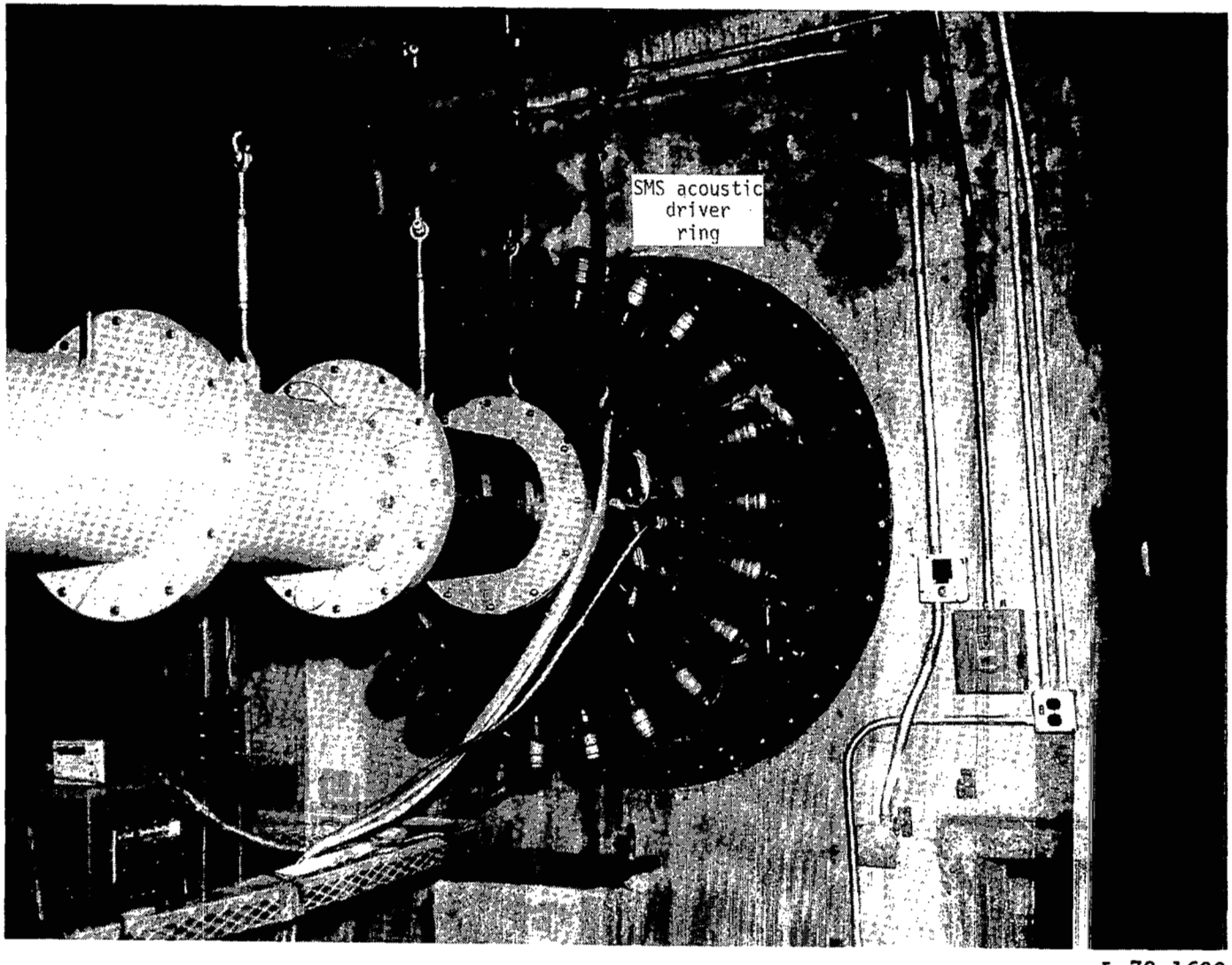

L-79-1699

Figure 6.- Photograph of spinning mode synthesizer.

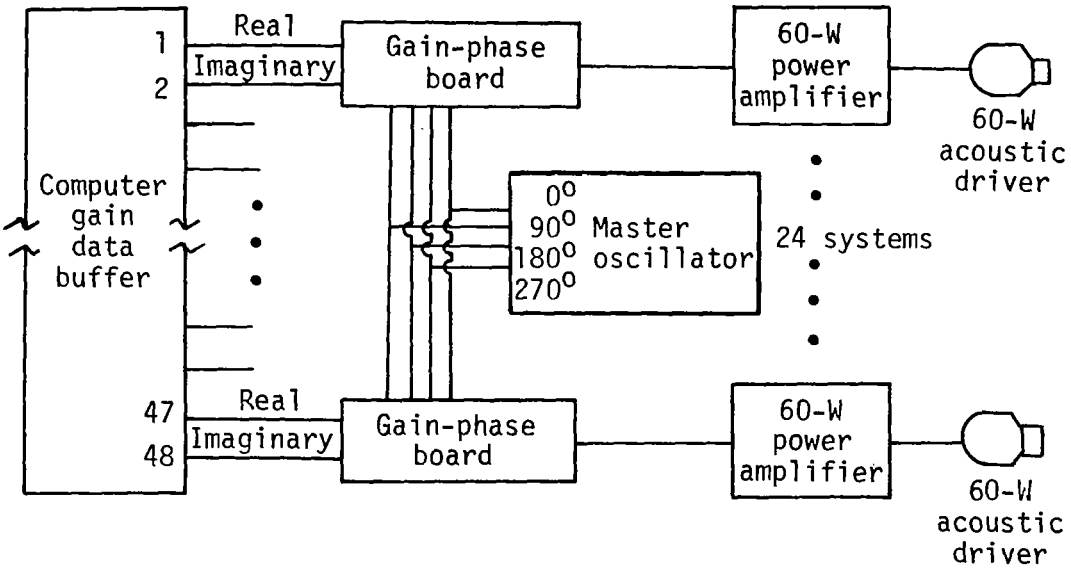

Figure 7.- Block diagram of driver excitation system.

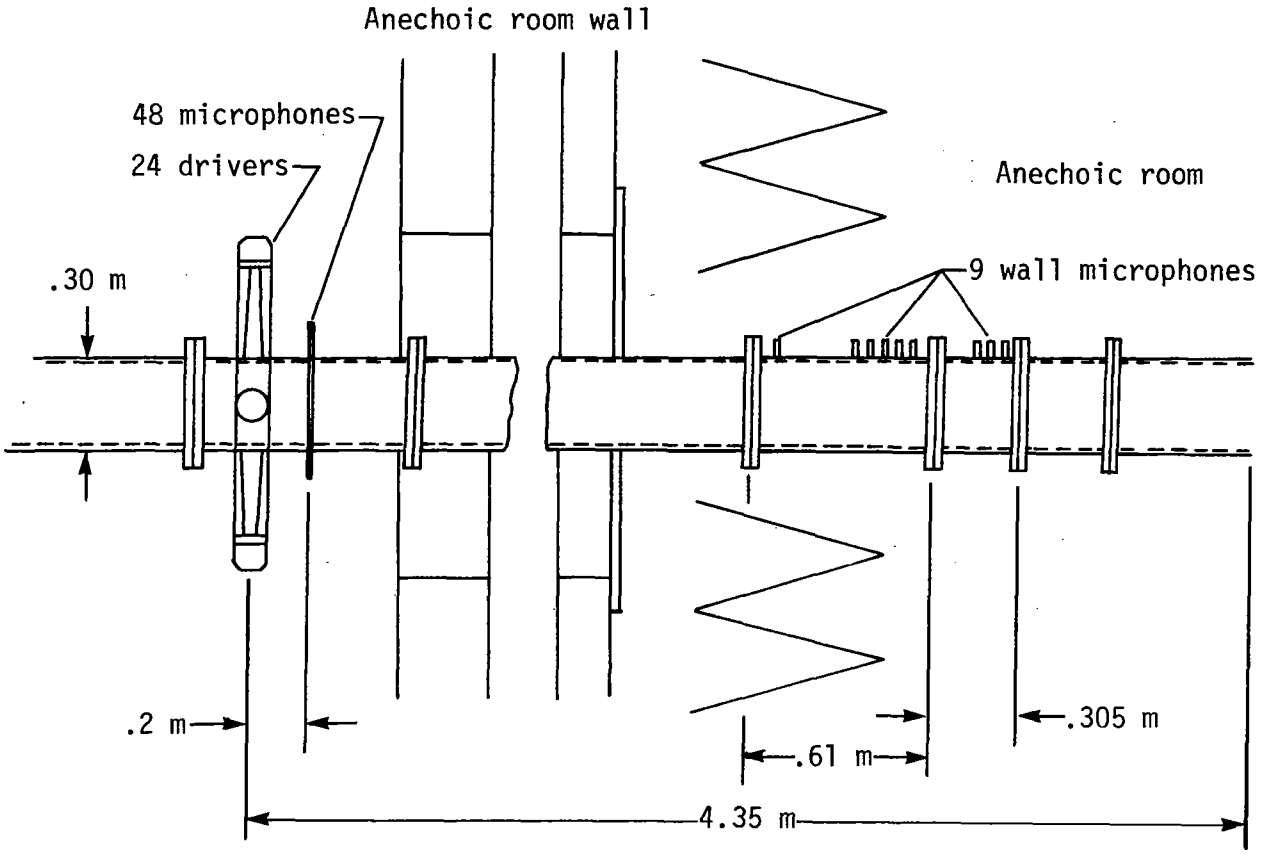

Figure 8.- Unflanged-duct test configuration.

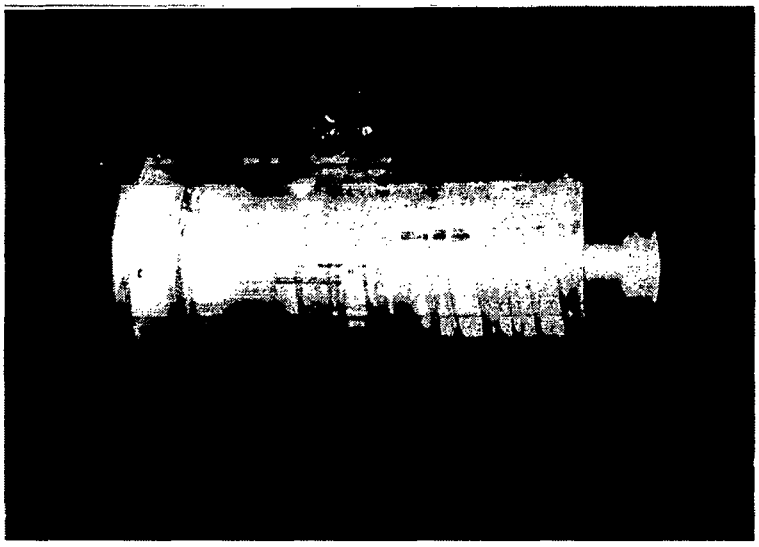

L-80-180

Figure 9.- Unflanged-duct inlet.

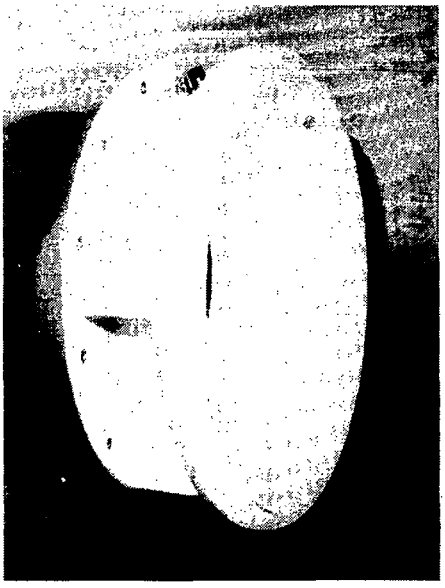

L-80-181

(a) Photograph.

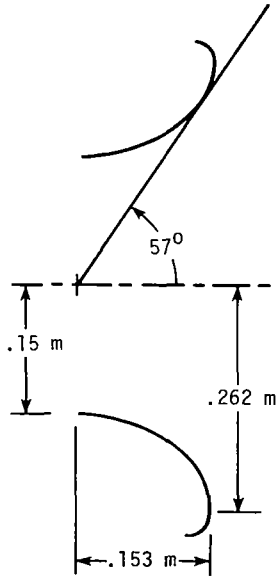

(b) Sectional view.

Figure 10.- Bellmouth inlet.

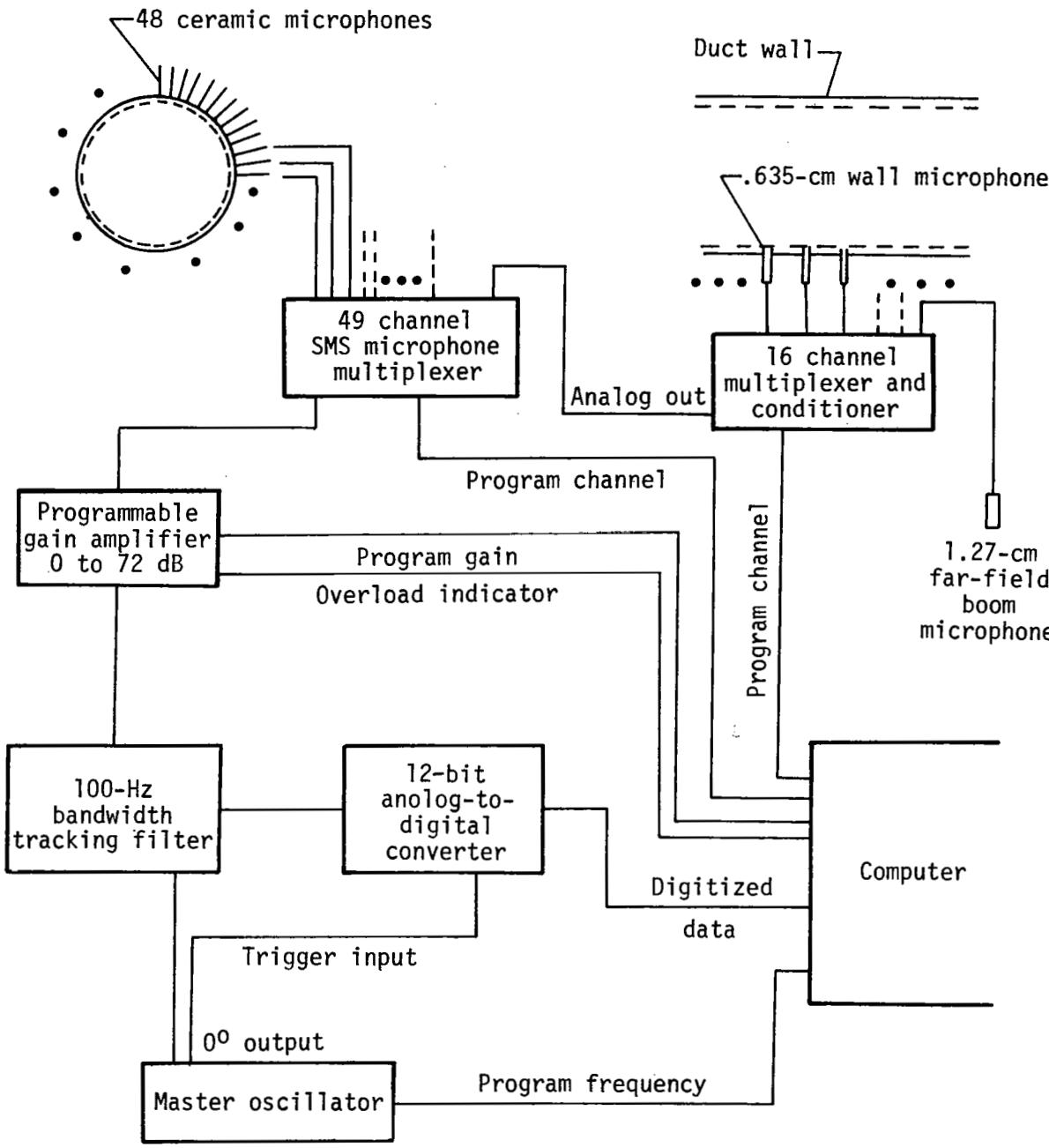

Figure 11.- Acoustic data acquisition system.

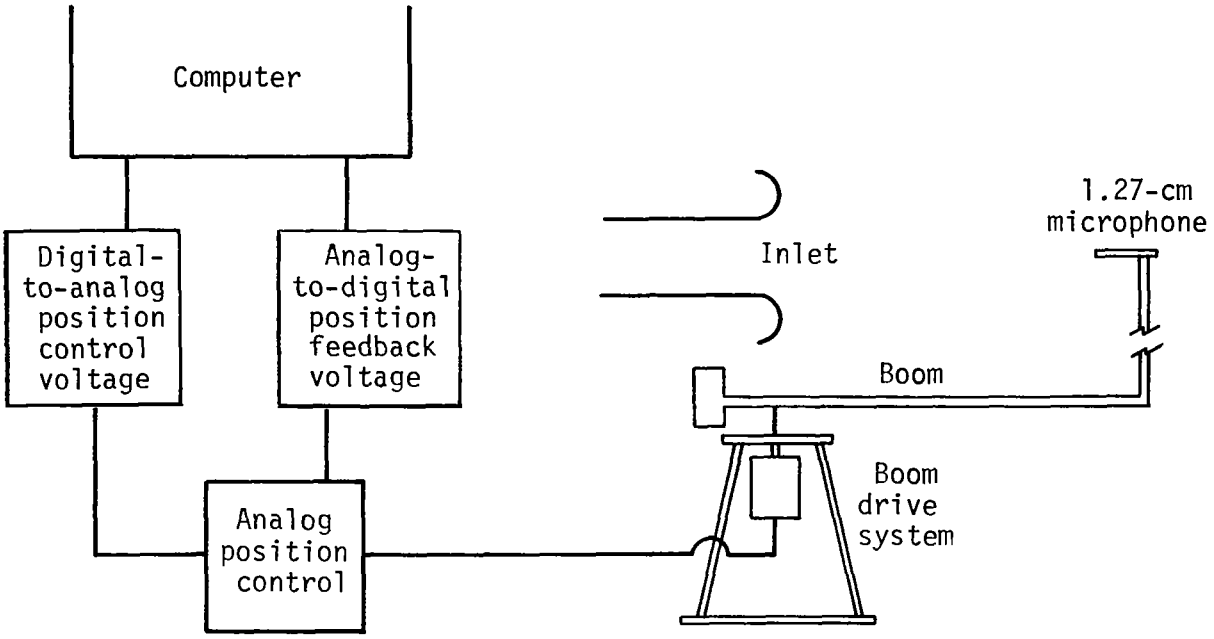

Figure 12.- Block diagram of far-field boom driver system.

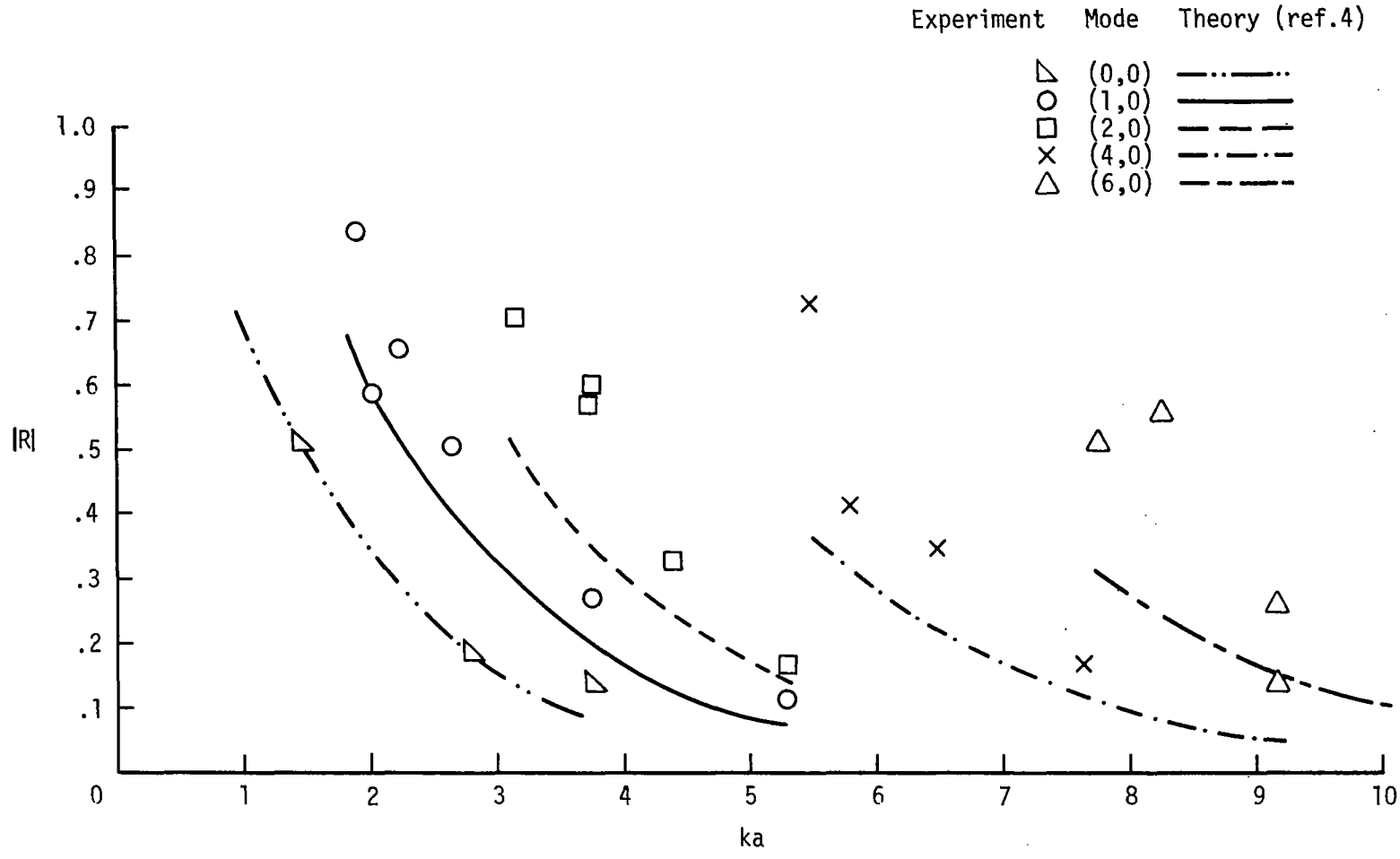

(a) Pressure reflection coefficient moduli.

Figure 13.- Comparison of measured and theoretical reflection coefficient with frequency parameter for unflanged duct.

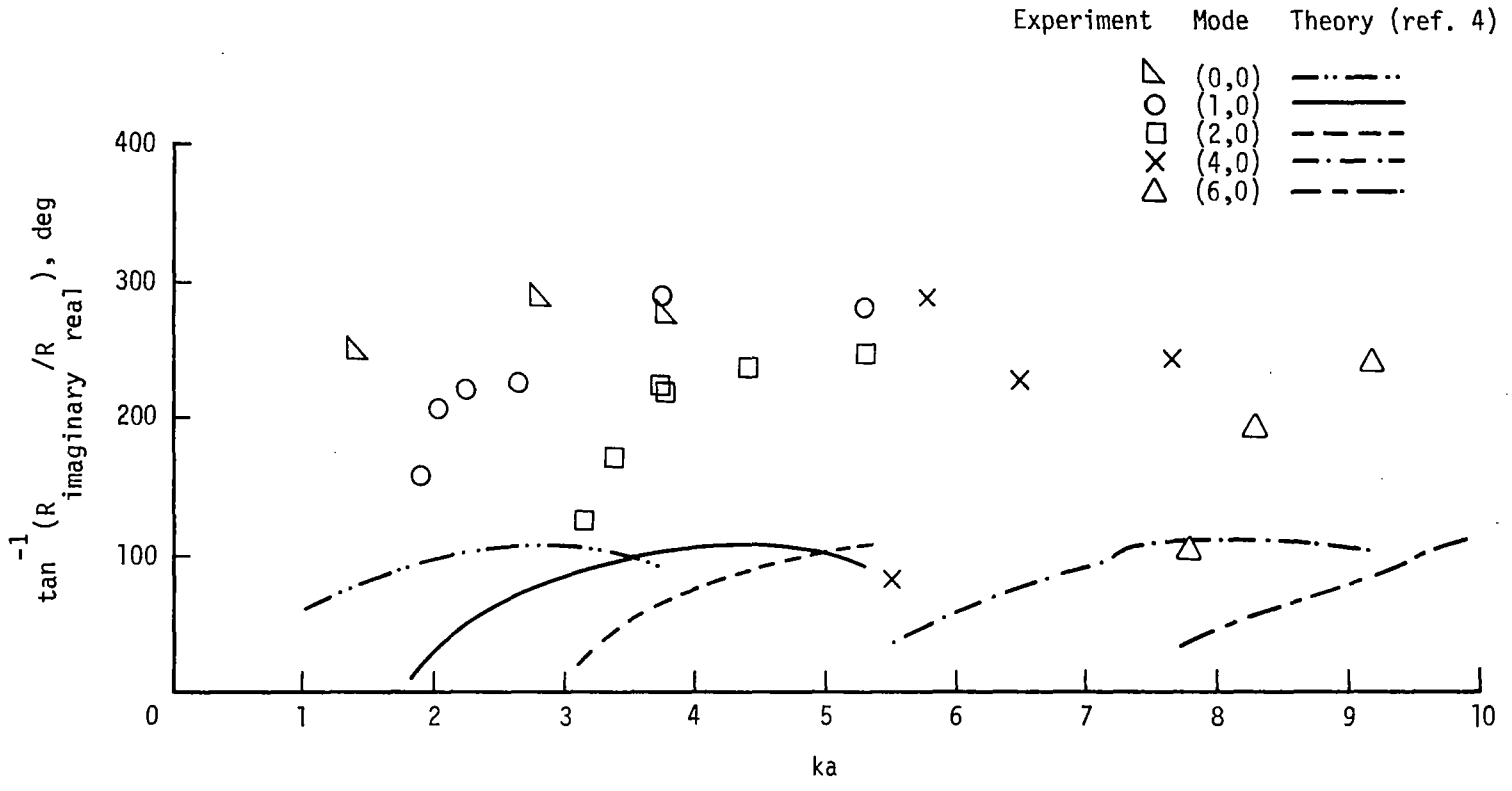

(b) Pressure reflection coefficient phase.

Figure 13.- Concluded.

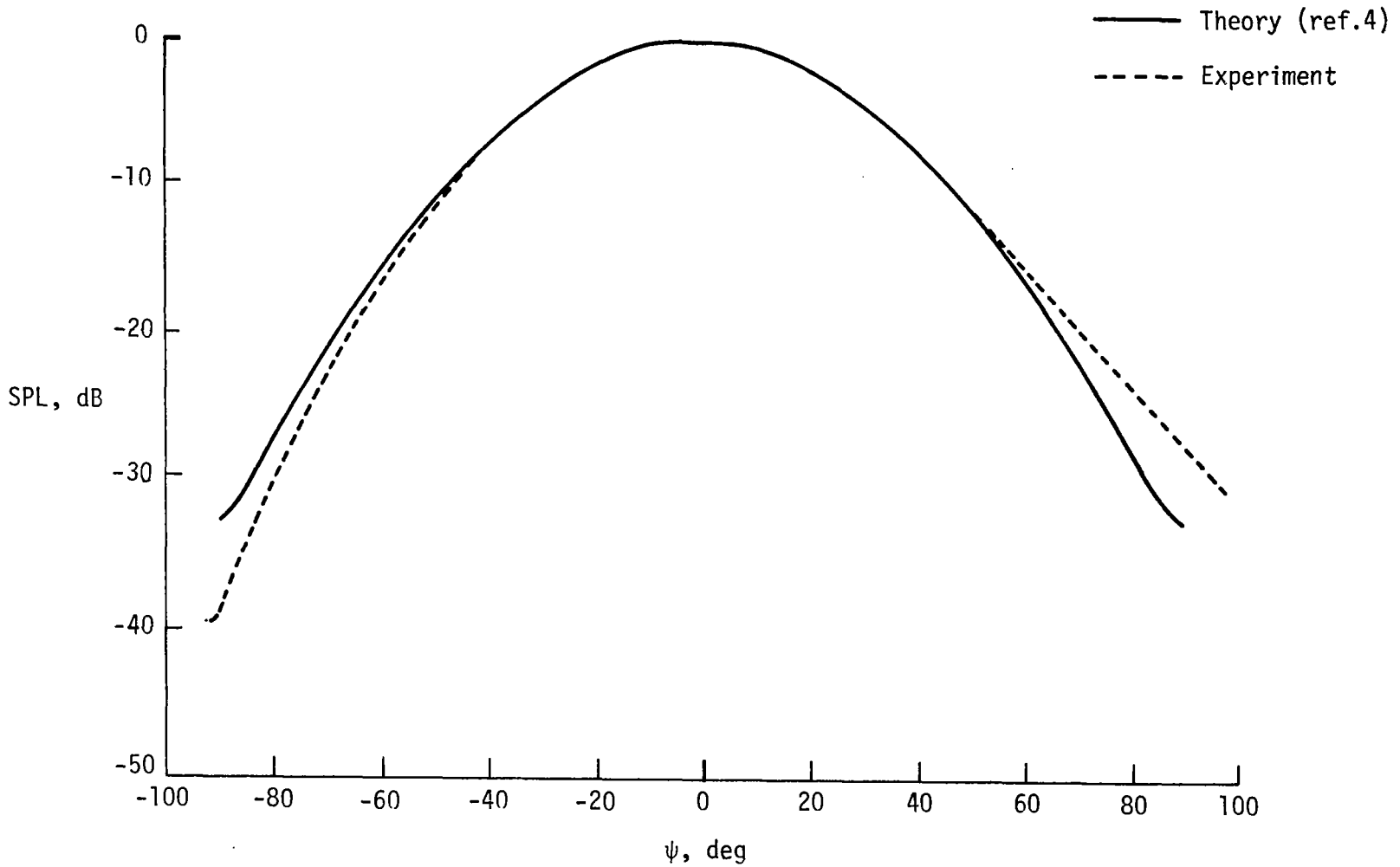

(a) Unflanged duct; ka = 3.76; mode (0,0).

Figure 14.- Comparison between theory and experiment of sound pressure level variation of radiated field against polar angle.

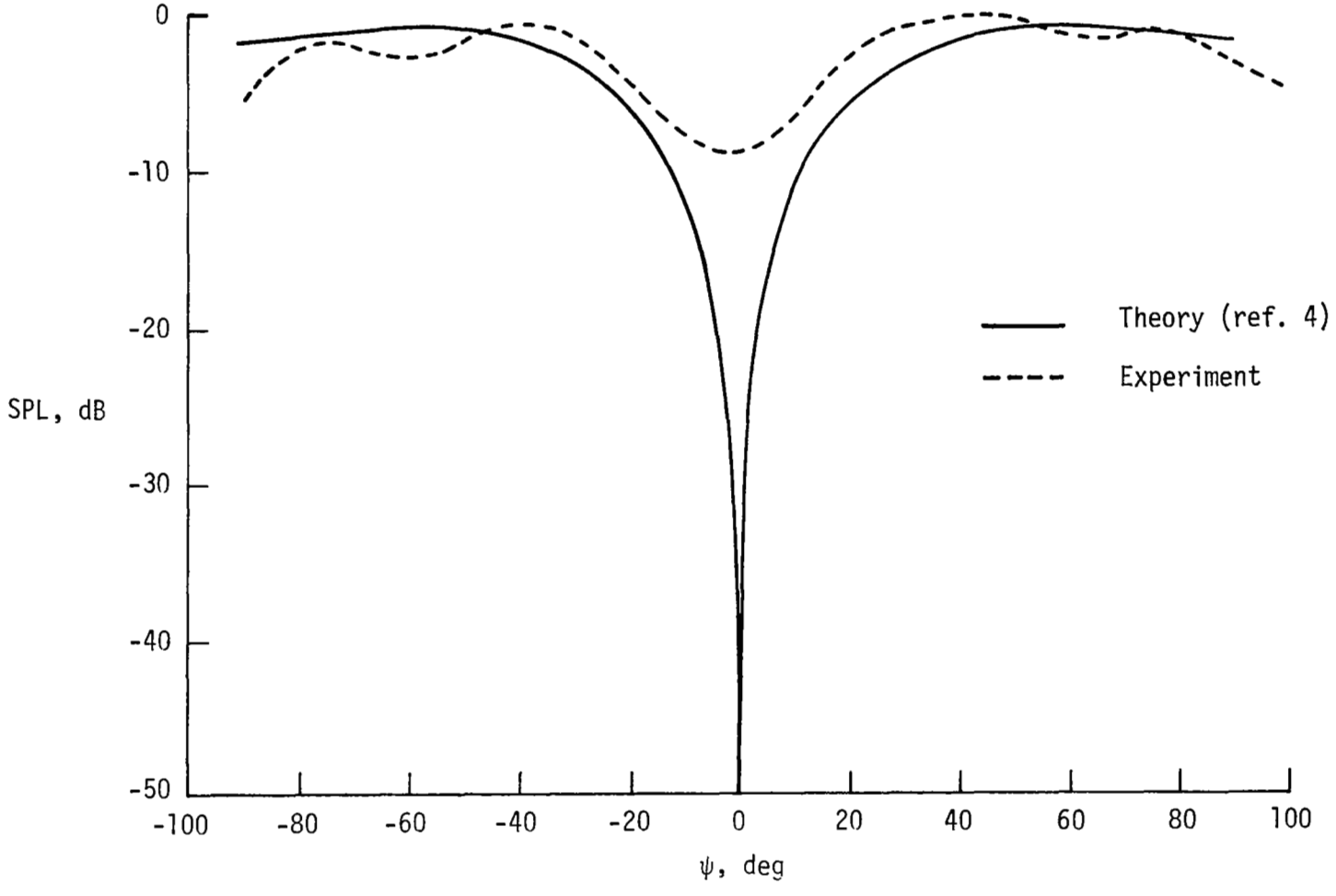

(b) Unflanged duct; ka = 2.03; f/f_{mn} = 1.11; mode (1,0).

Figure 14.- Continued.

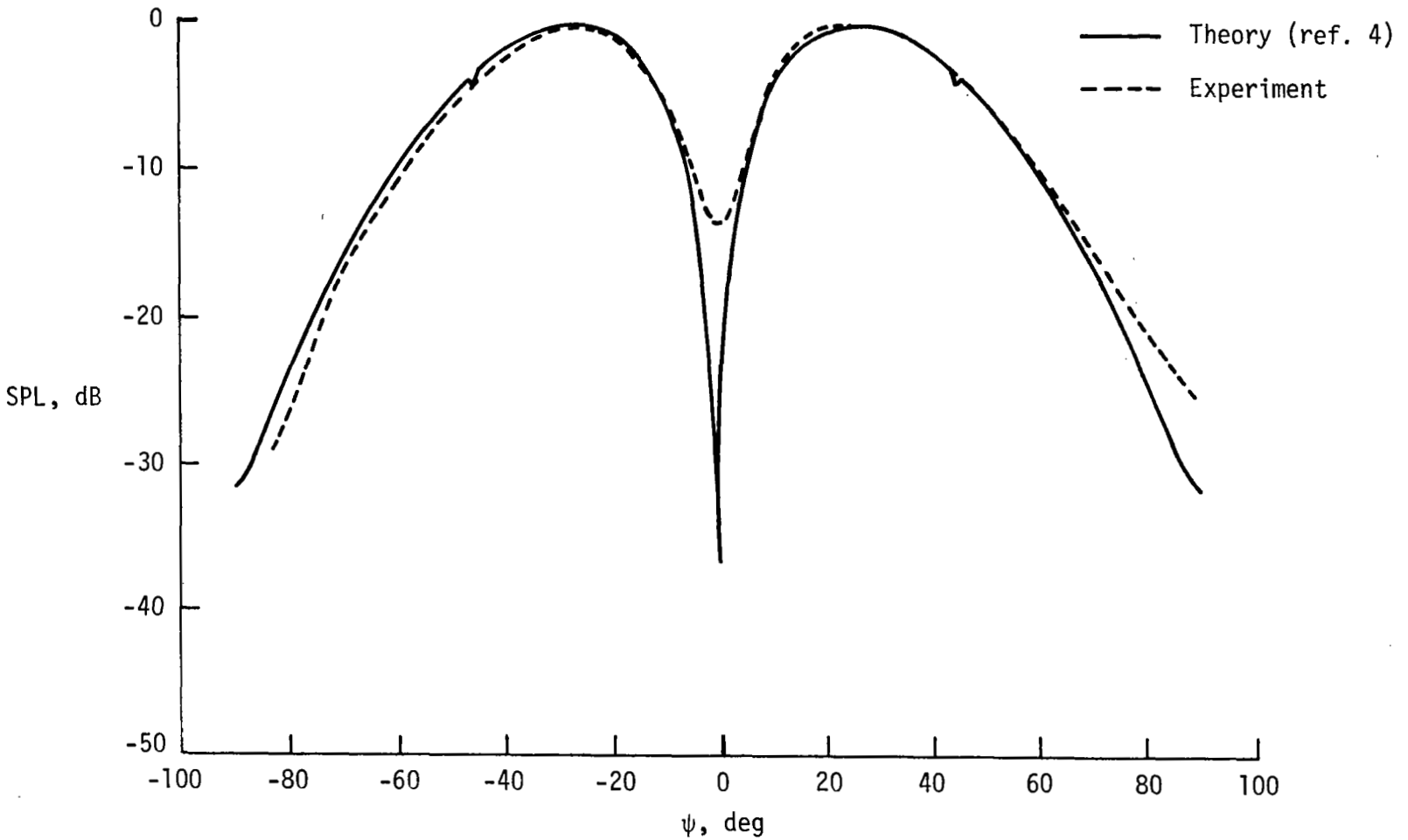

(c) Unflanged duct; ka = 5.29; f/f_{mn} = 2.87; mode (1,0).

Figure 14.- Continued.

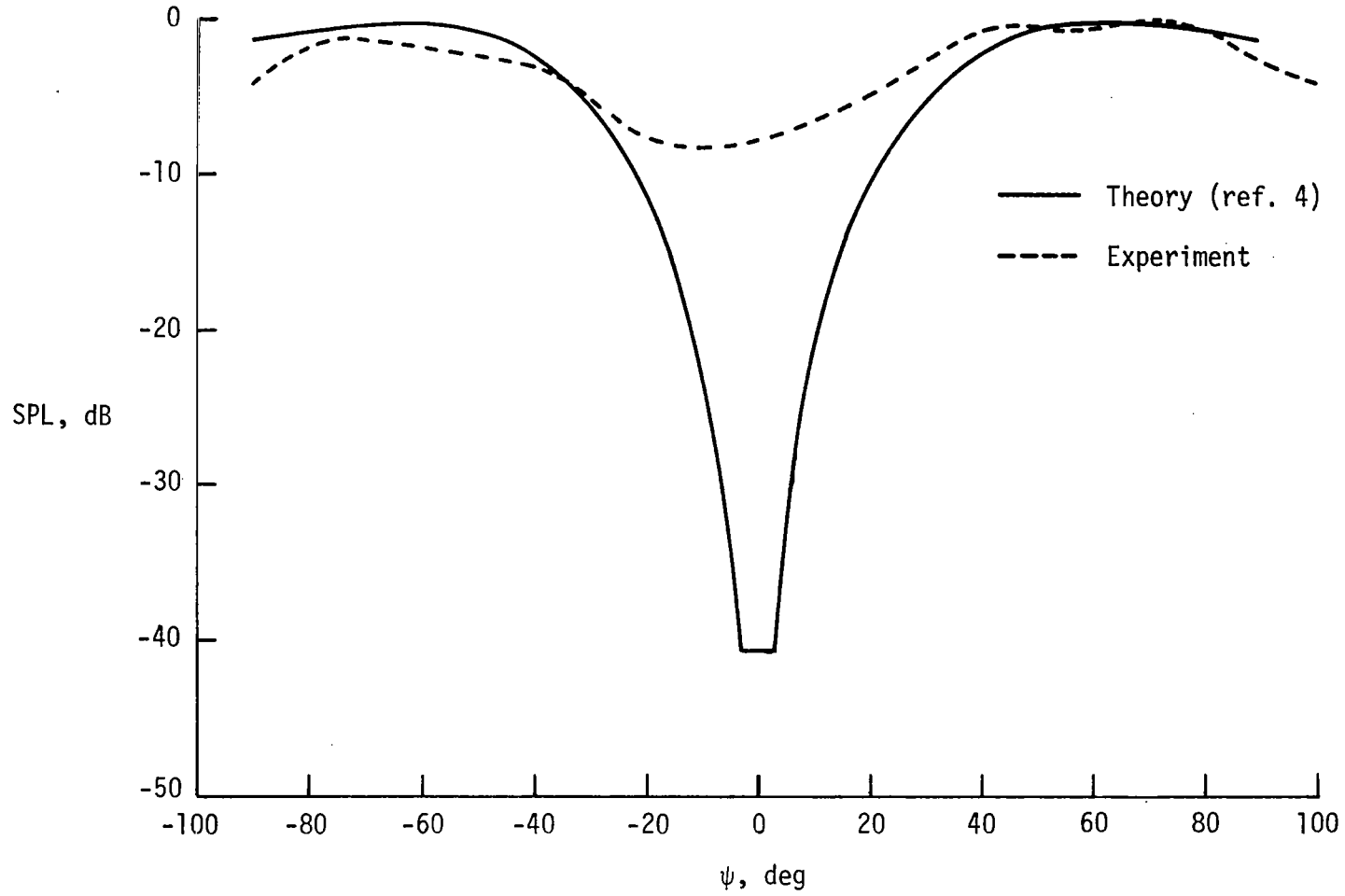

(d) Unflanged duct; ka = 3.37; f/f_{mn} = 1.11; mode (2,0).

Figure 14.- Continued.

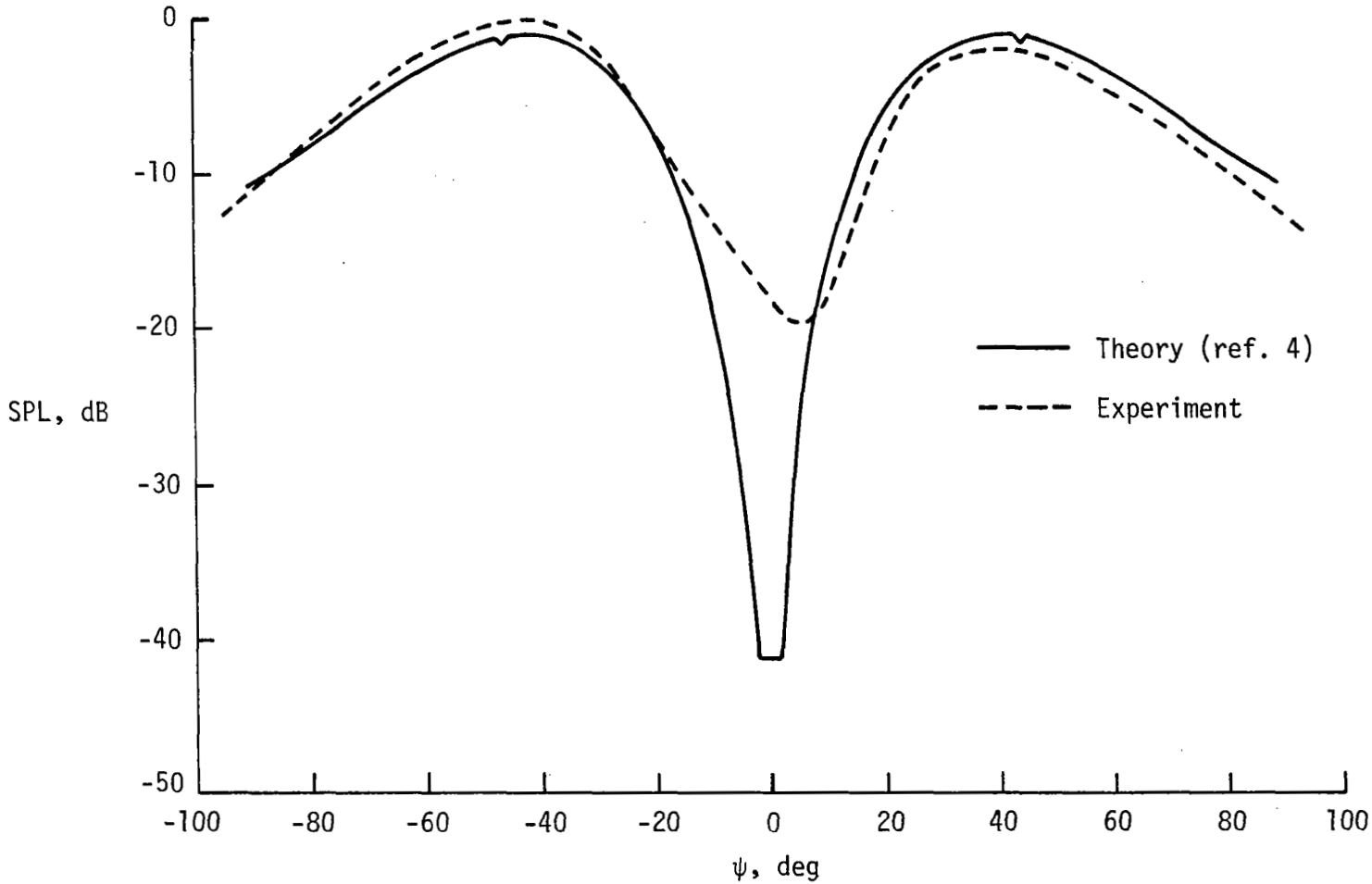

(e) Unflanged duct; ka = 5.29; f/f_{mn} = 1.74; mode (2,0).

Figure 14.- Continued.

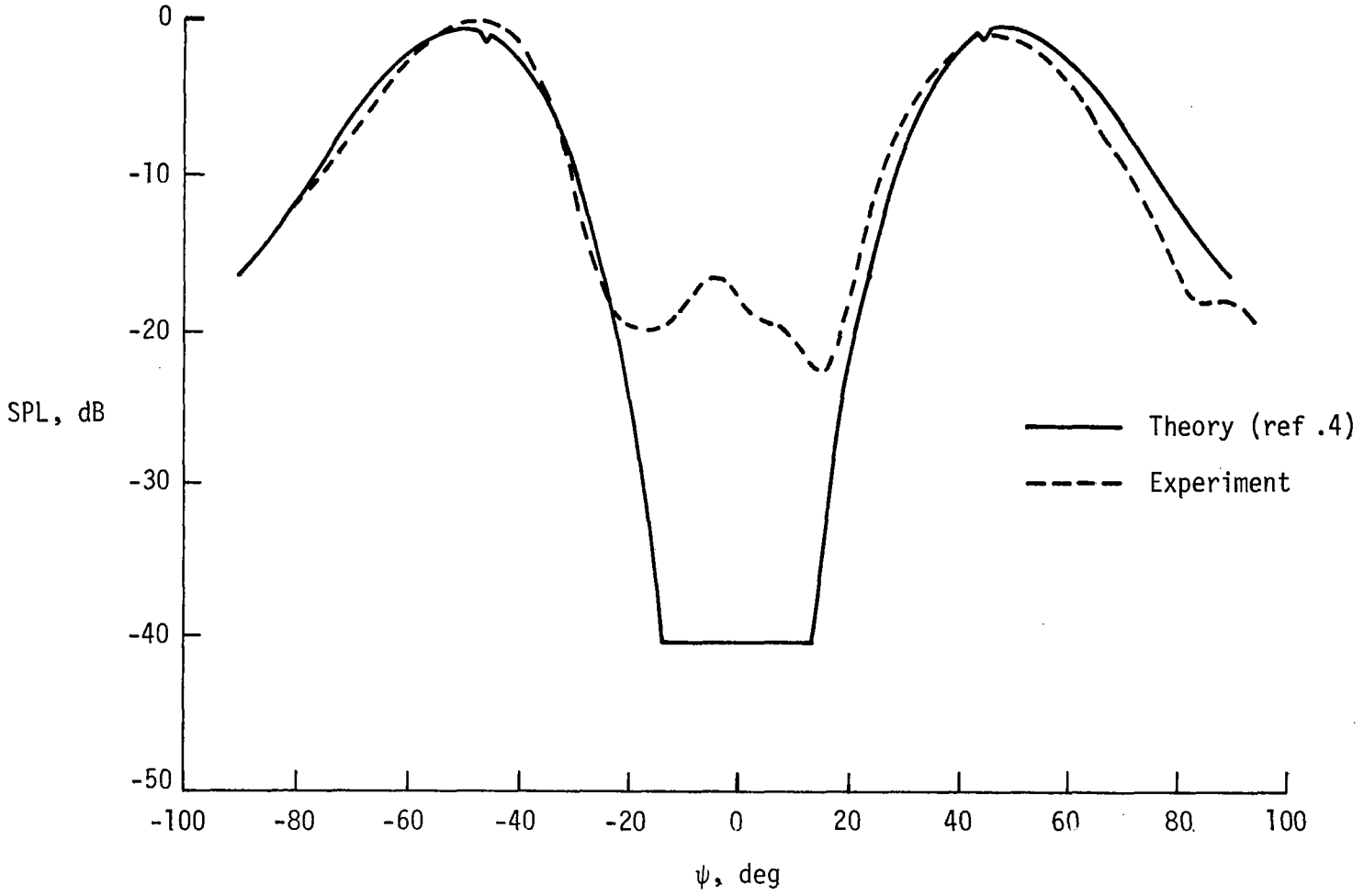

(f) Unflanged duct; ka = 11.14; f/f_{mn} = 1.49; mode (6,0).

Figure 14.- Concluded.

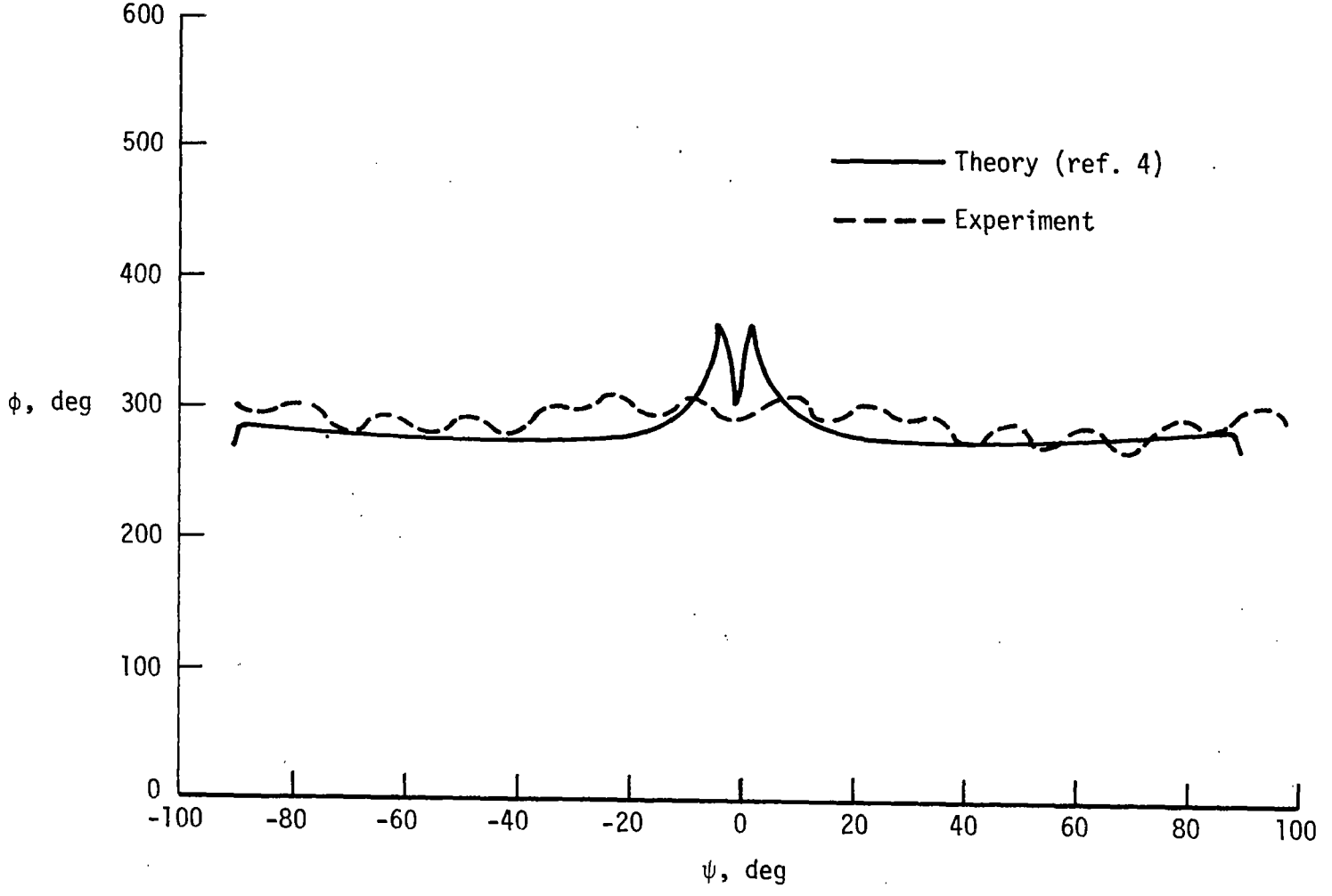

(a) Unflanged duct; ka = 1.39; mode (0,0).

Figure 15.- Comparison between theory and experiment of phase variation of radiated field against polar angle.

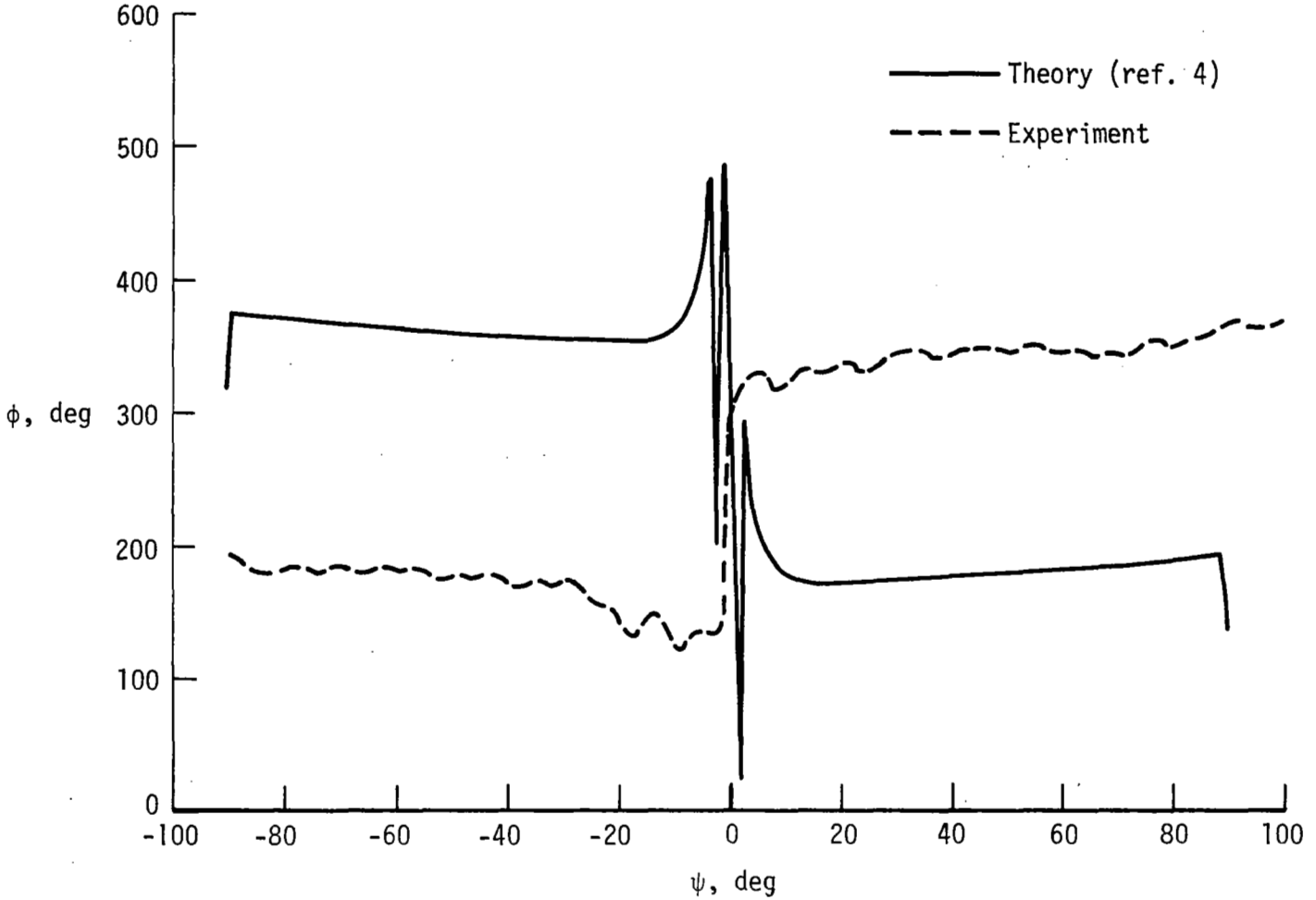

(b) Unflanged duct; ka = 2.66; mode (1,0).

Figure 15.- Concluded.

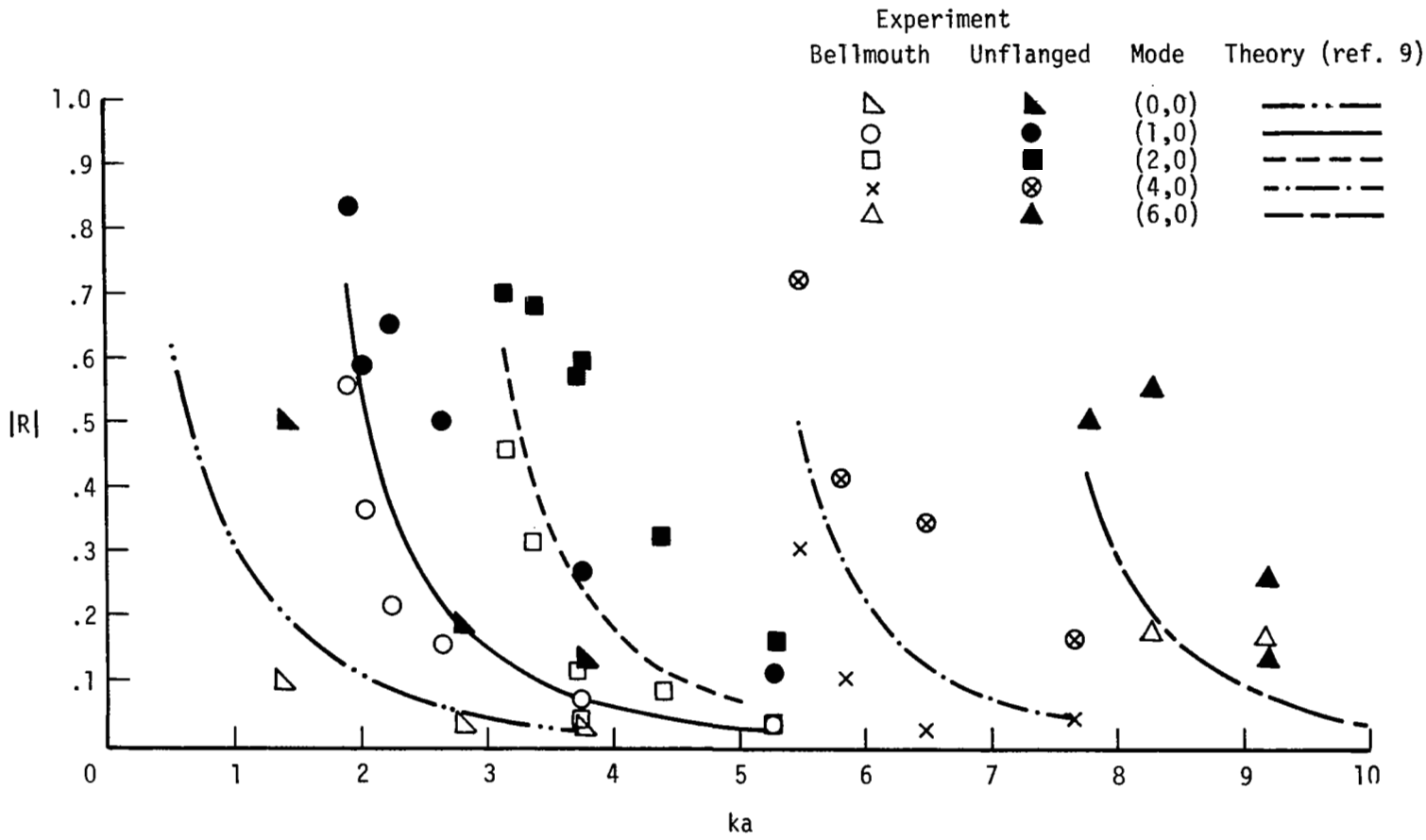

(a) Pressure reflection coefficient moduli.

Figure 16.- Comparison of measured and theoretical reflection coefficients plotted against frequency parameter for bellmouth inlet without flow and measured values for unflanged duct.

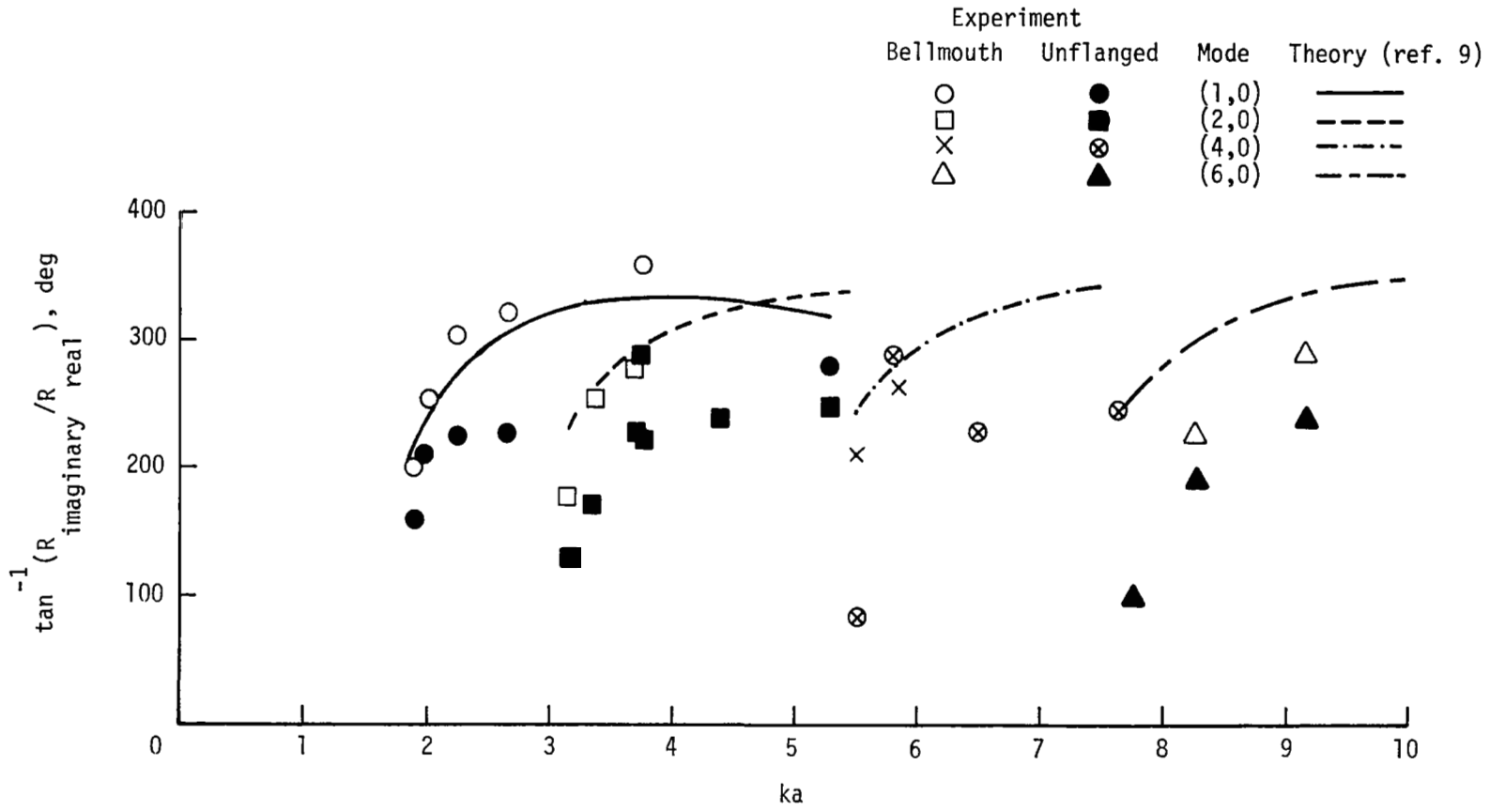

(b) Pressure reflection coefficient phase.

Figure 16.- Concluded.

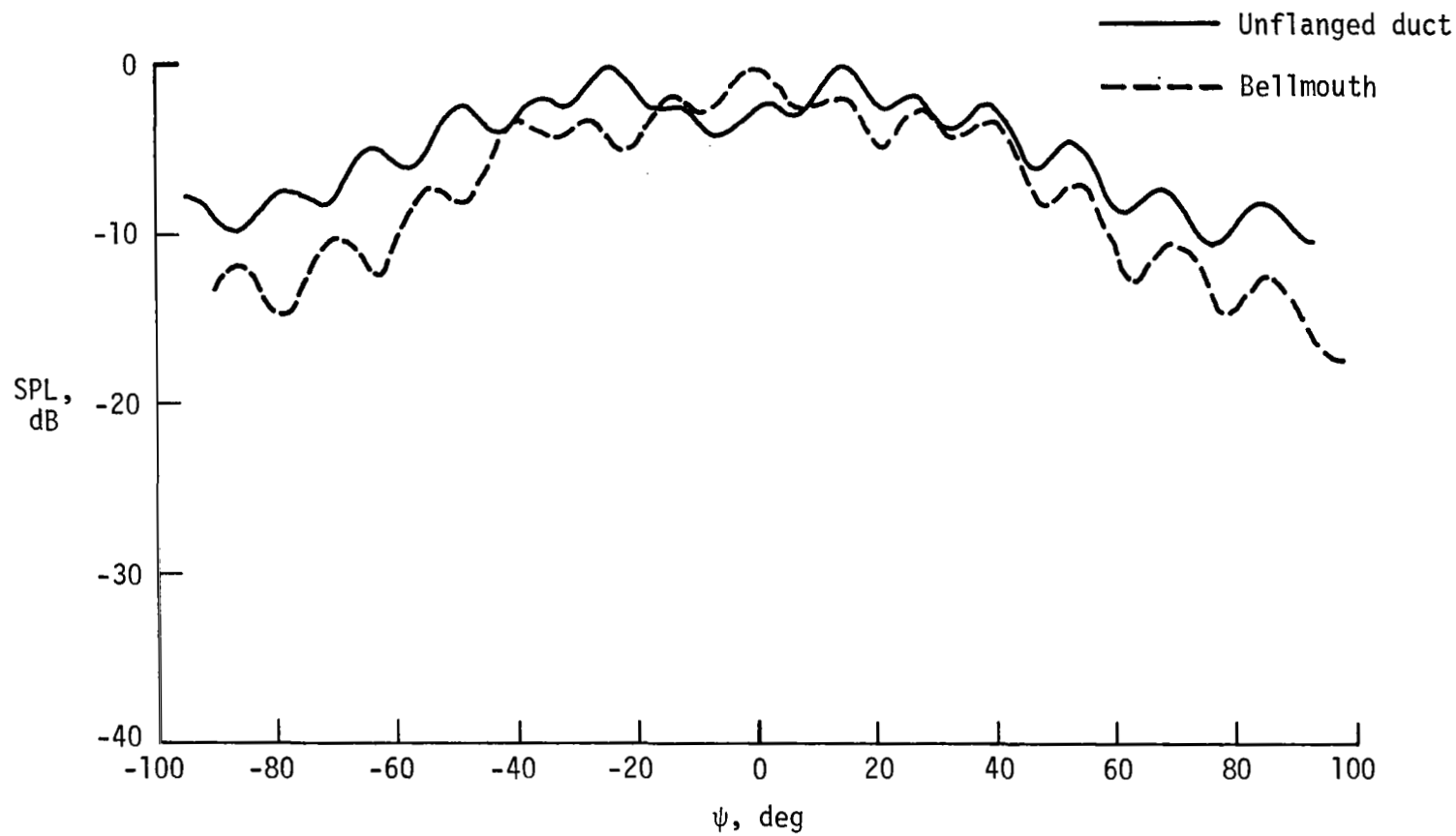

(a) Mode (0,0); ka = 1.39; M = 0.

Figure 17.- Influence of inlet geometry on sound pressure level variation of radiated field with polar angle.

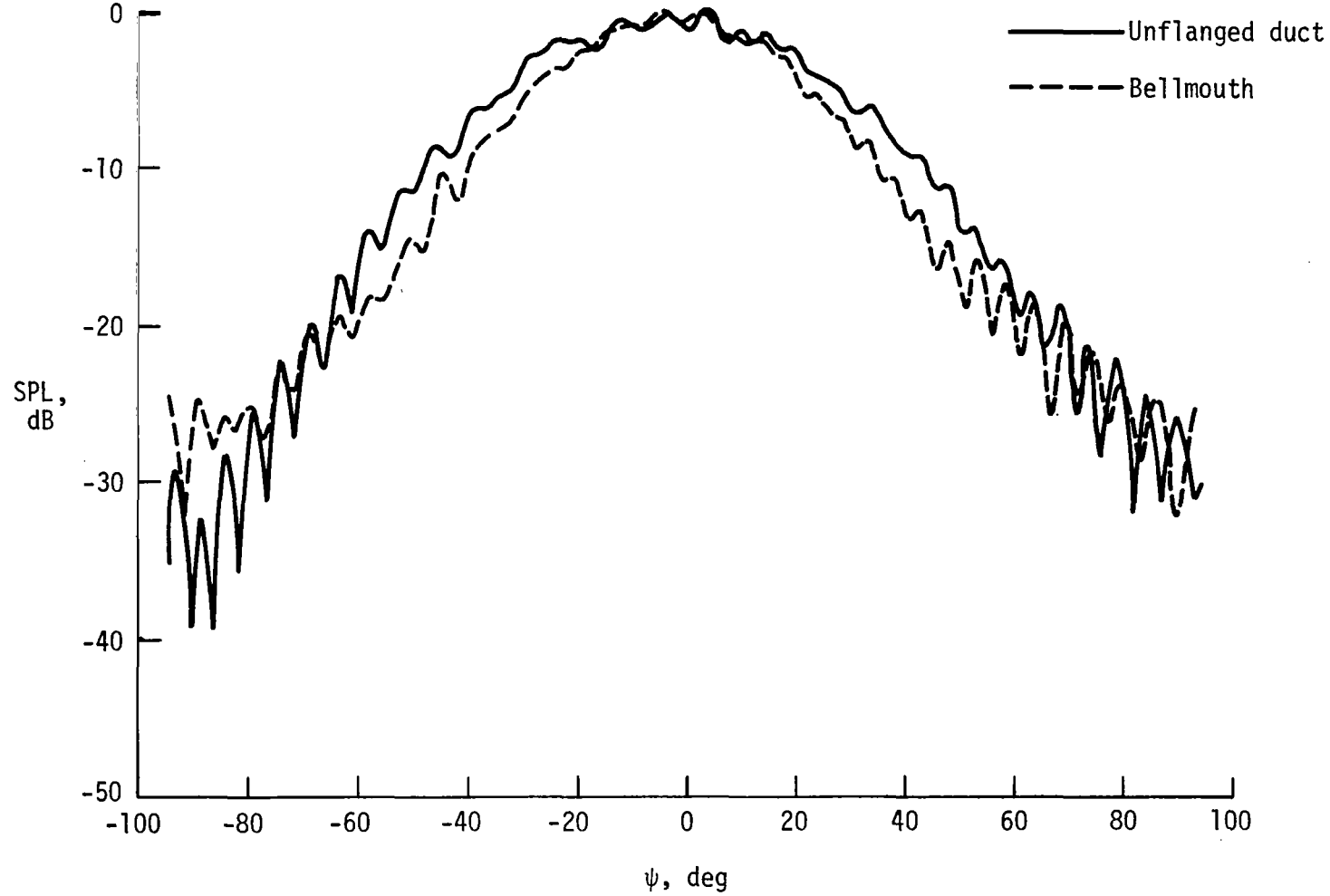

(b) Mode (0,0); ka = 3.76; M = 0.

Figure 17.- Continued.

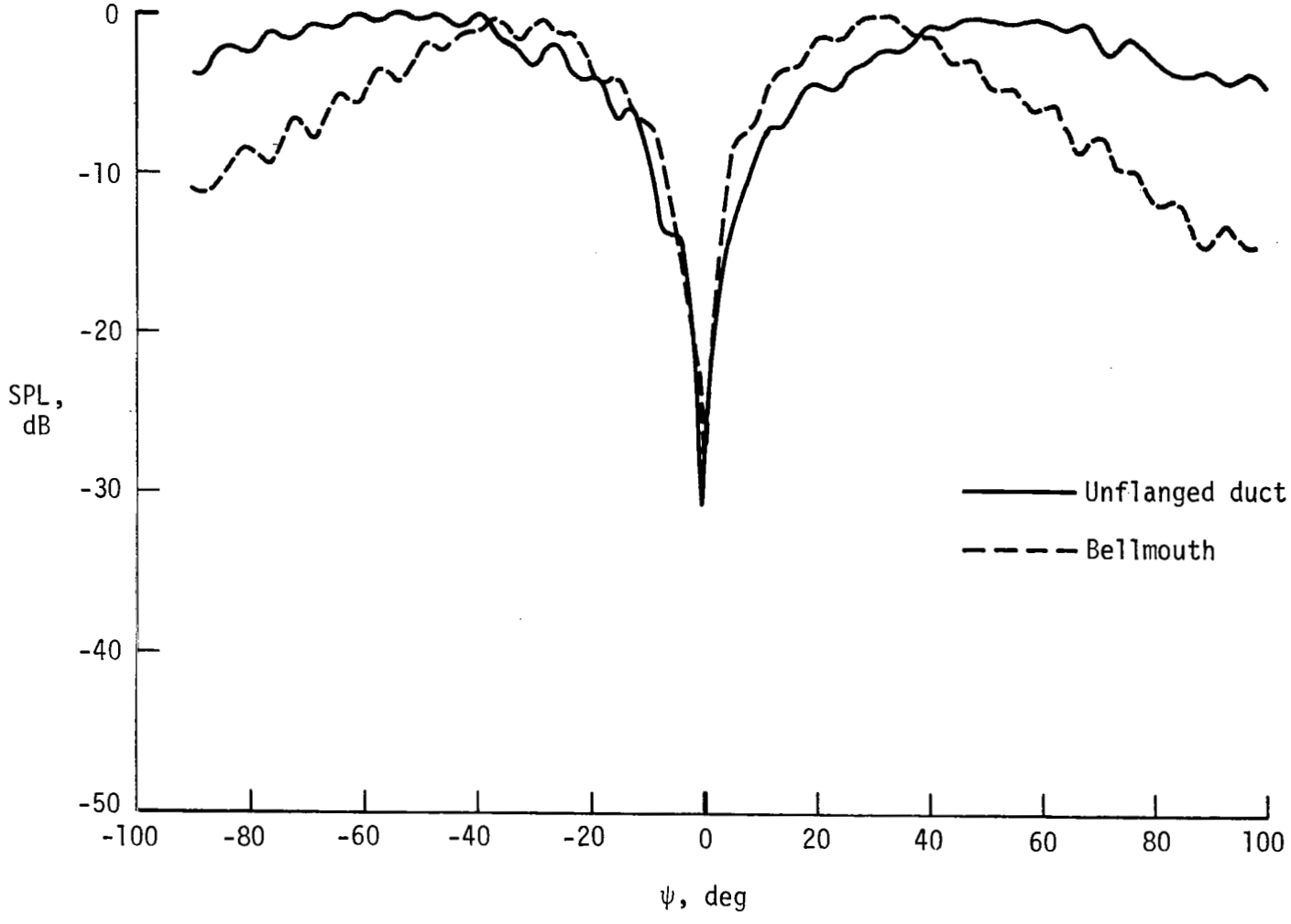

(c) Mode (1,0); ka = 2.66; f/f_{mn} = 1.44; M = 0.

Figure 17.- Continued.

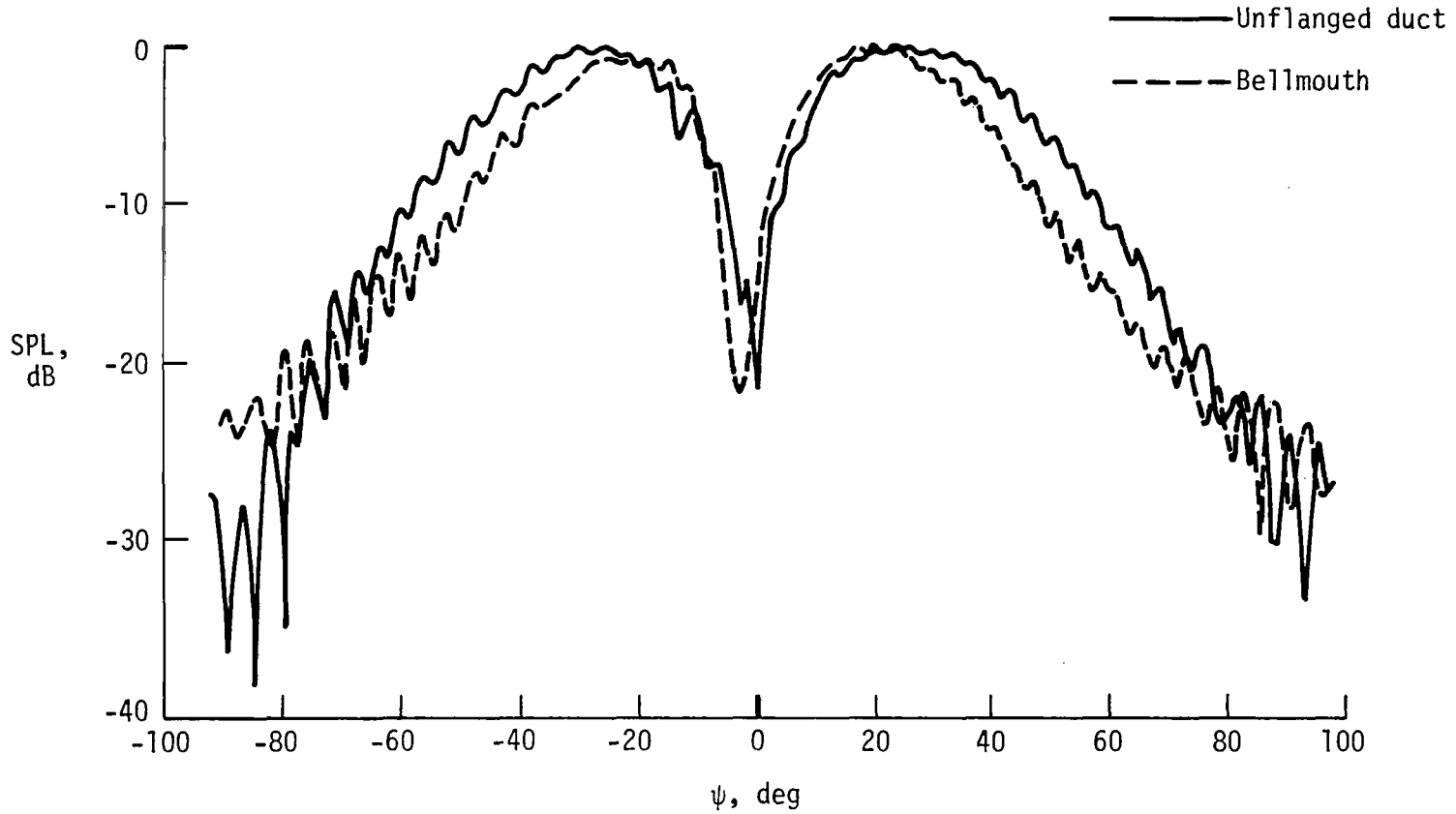

(d) Mode (1,0); ka = 5.29; f/f_{mn} = 2.87; M = 0.

Figure 17.- Concluded.

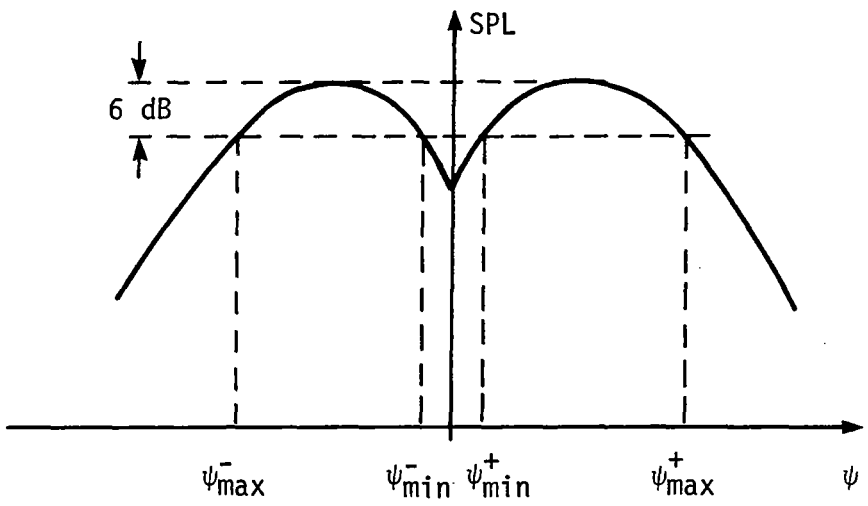

Figure 18.- Concept of angular location of predominant acoustic radiation.

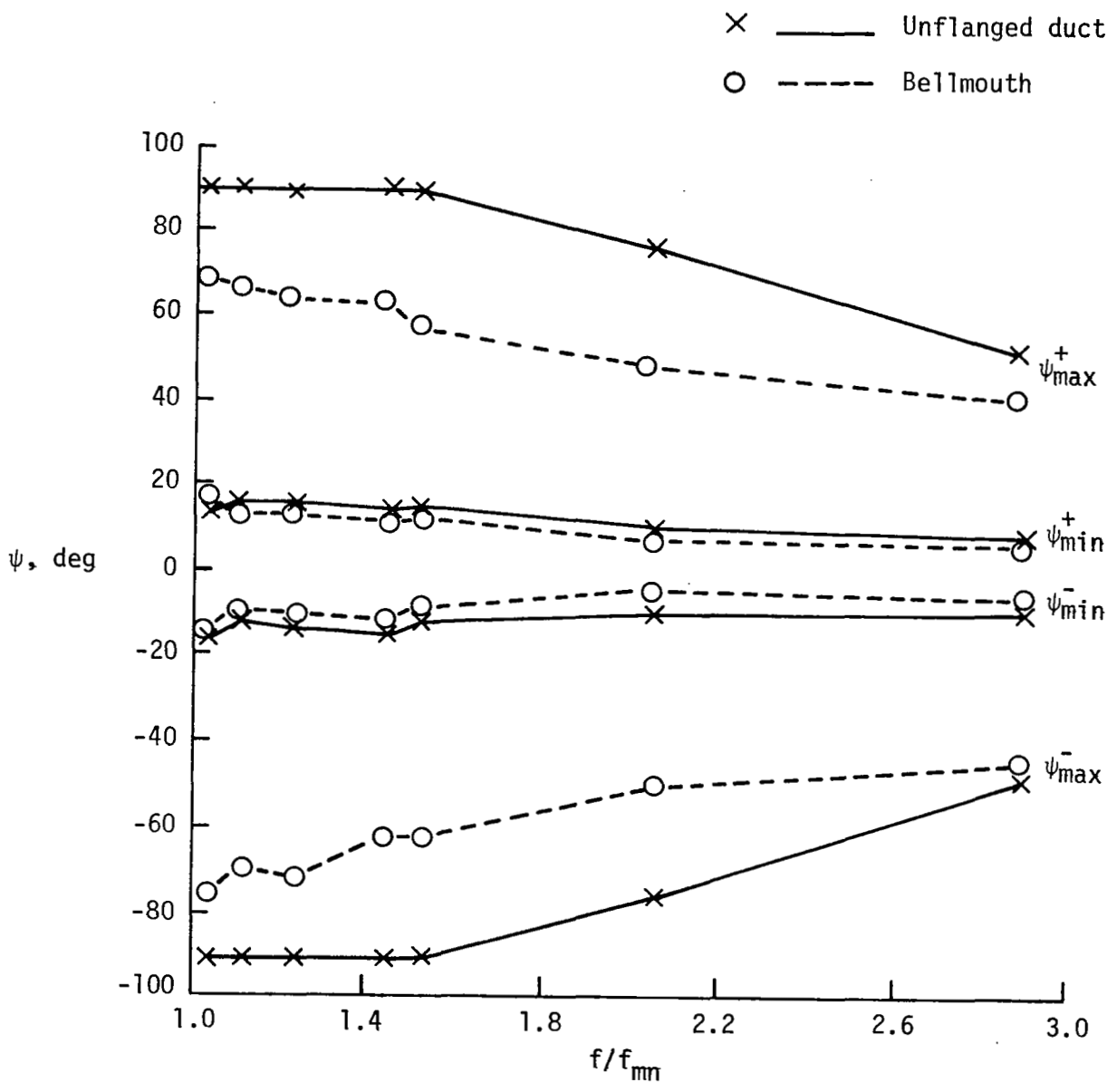

(a) Mode (1,0); M = 0.

Figure 19.- Effect of inlet geometry on principal lobes of radiation.

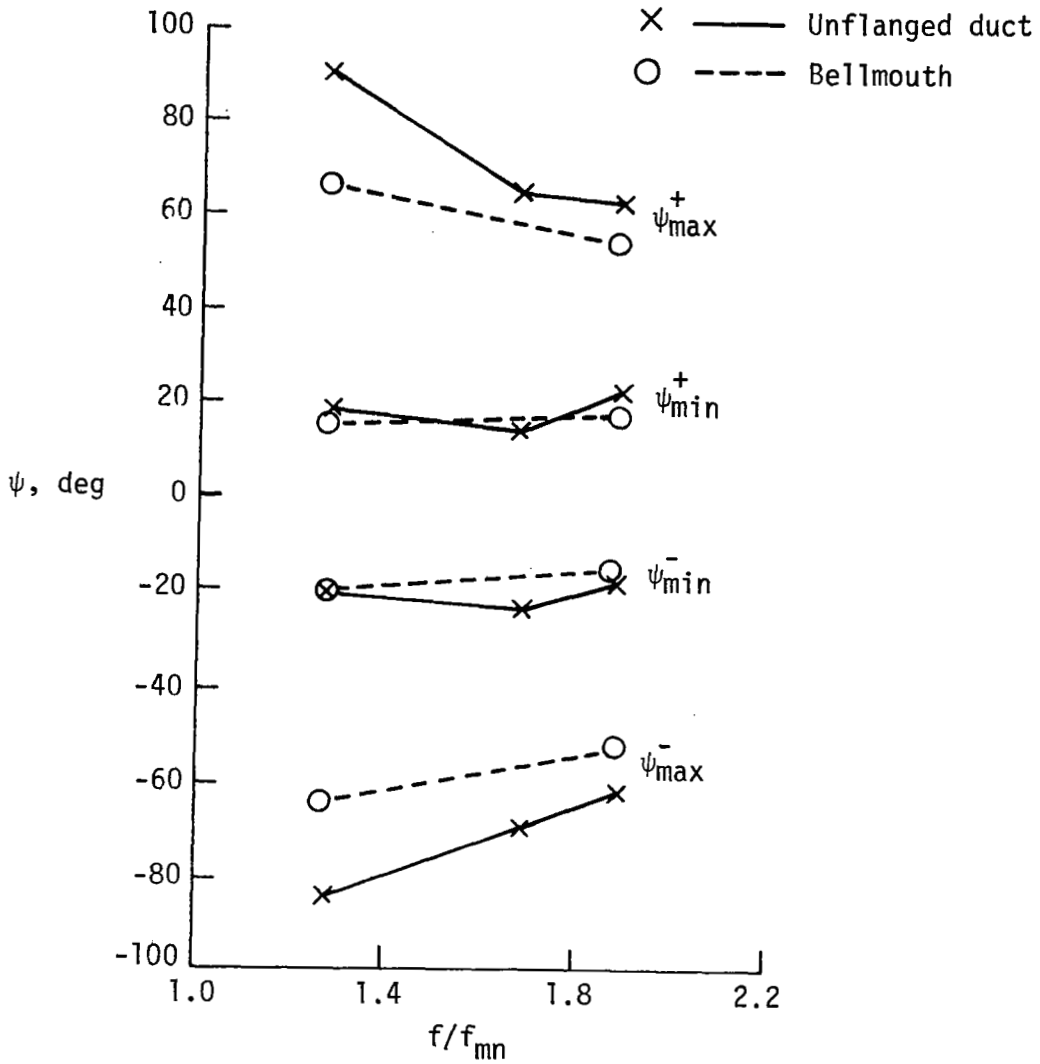

(b) Mode (3,0); M = 0.

Figure 19.- Continued.

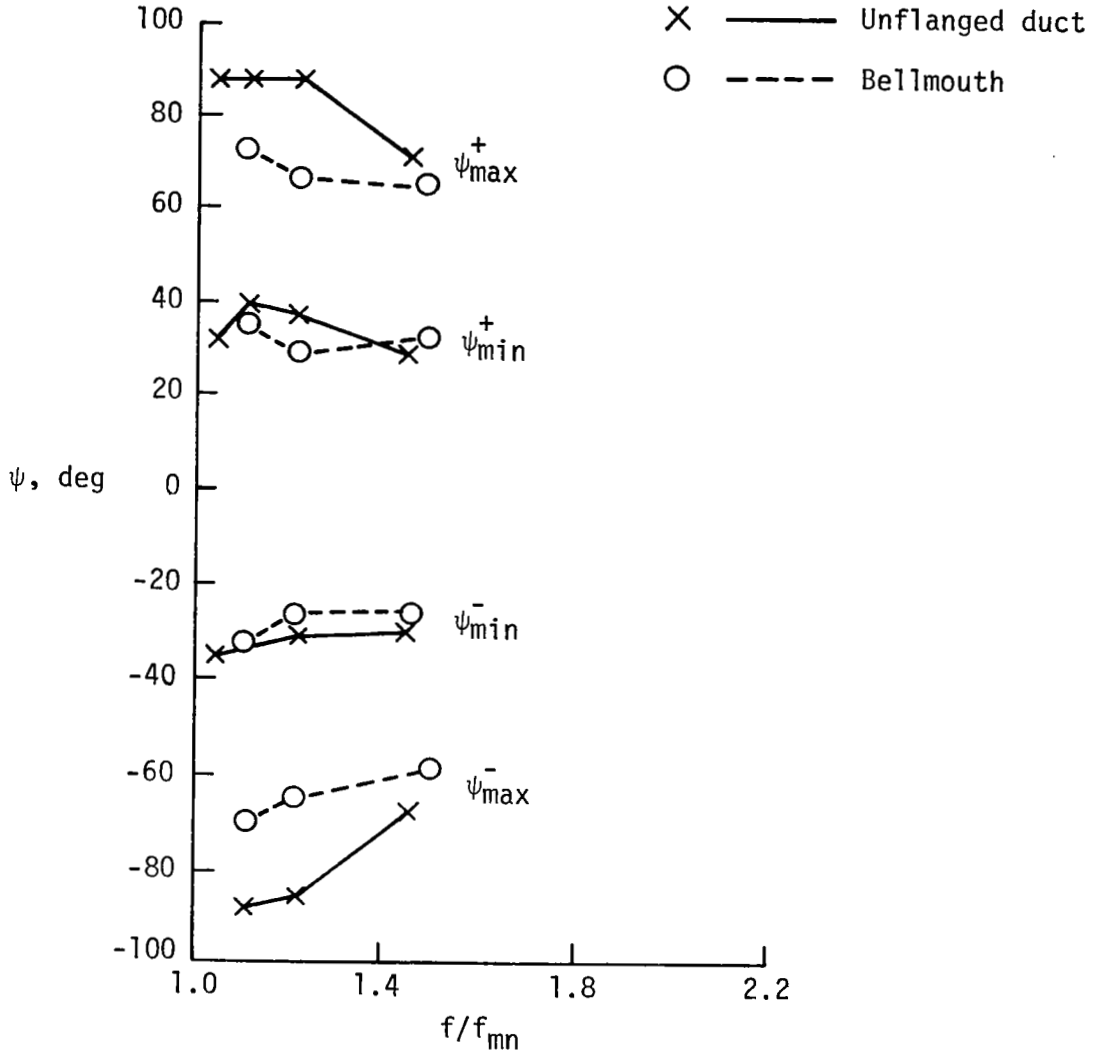

(c) Mode (6,0); M = 0.

Figure 19.- Concluded.

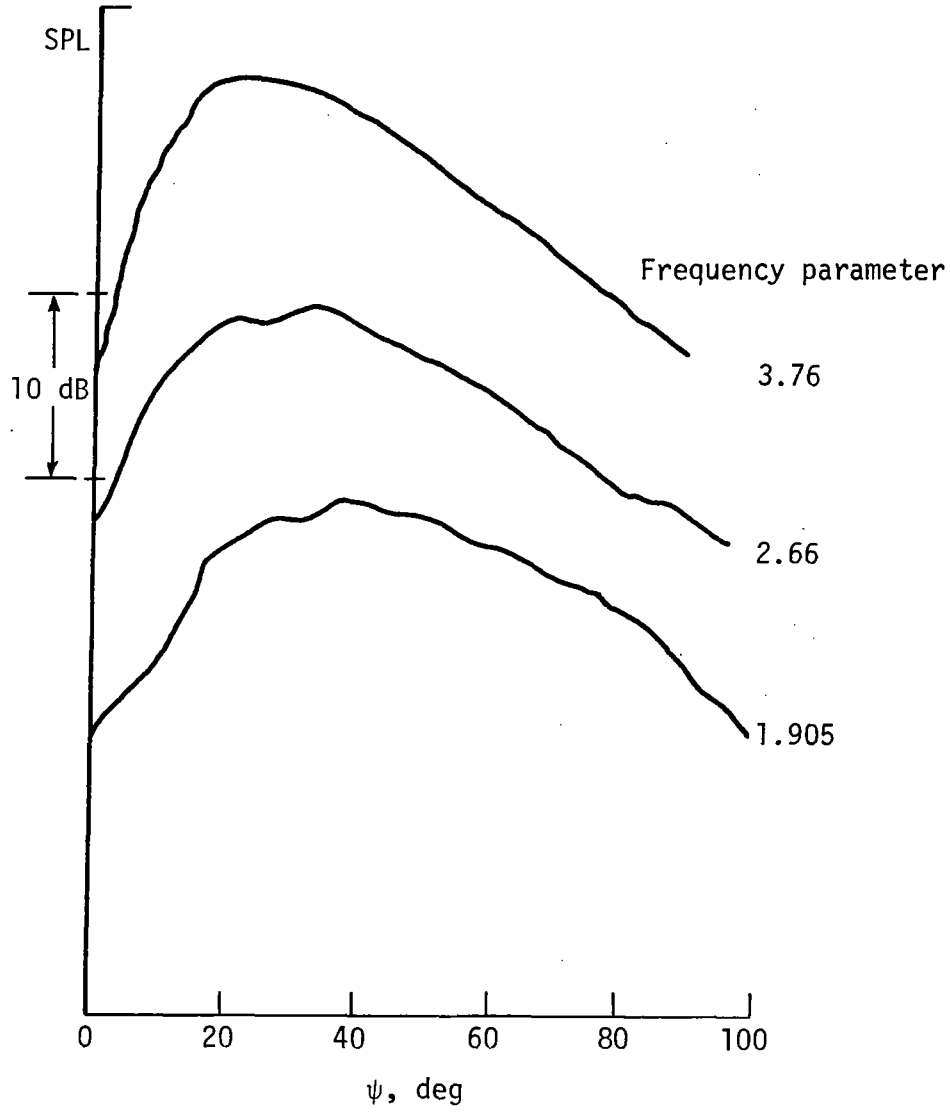

(a) Mode (1,0); M = 0.

Figure 20.- Influence of frequency on radiation pattern of bellmouth without flow.

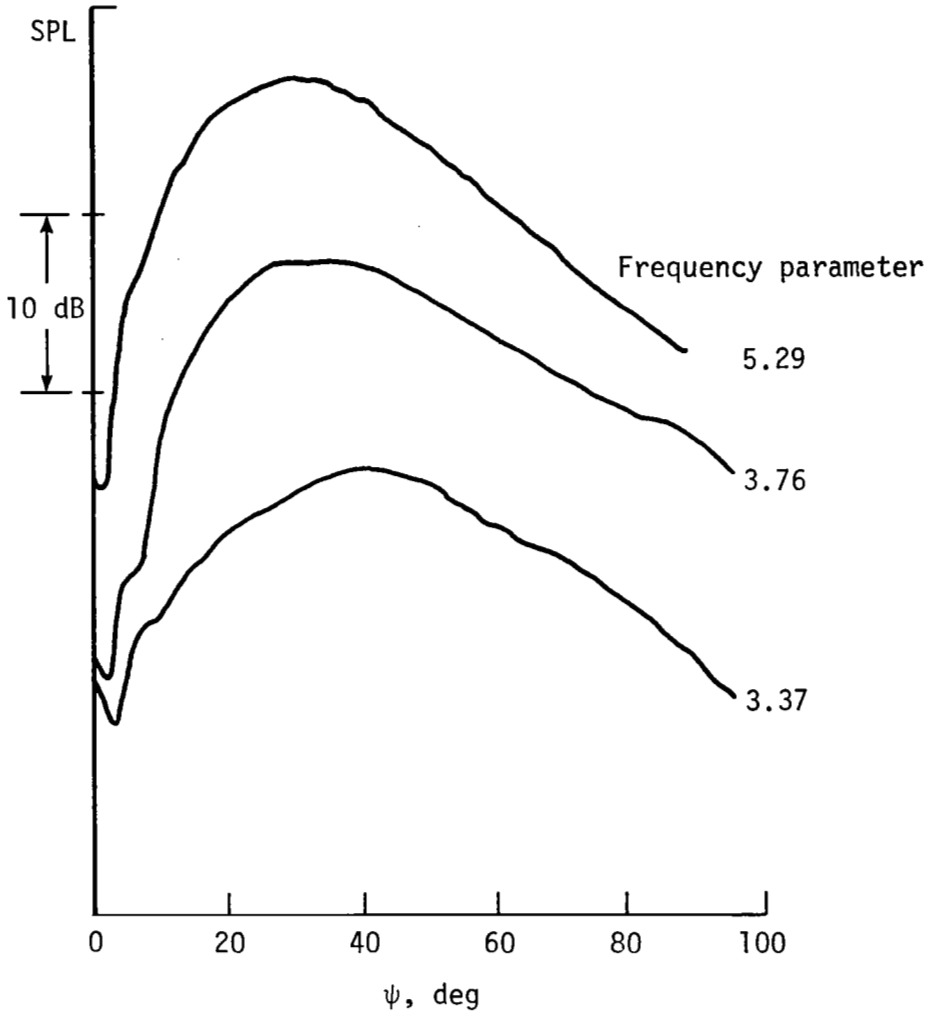

(b) Mode (2,0); M = 0.

Figure 20.- Concluded.

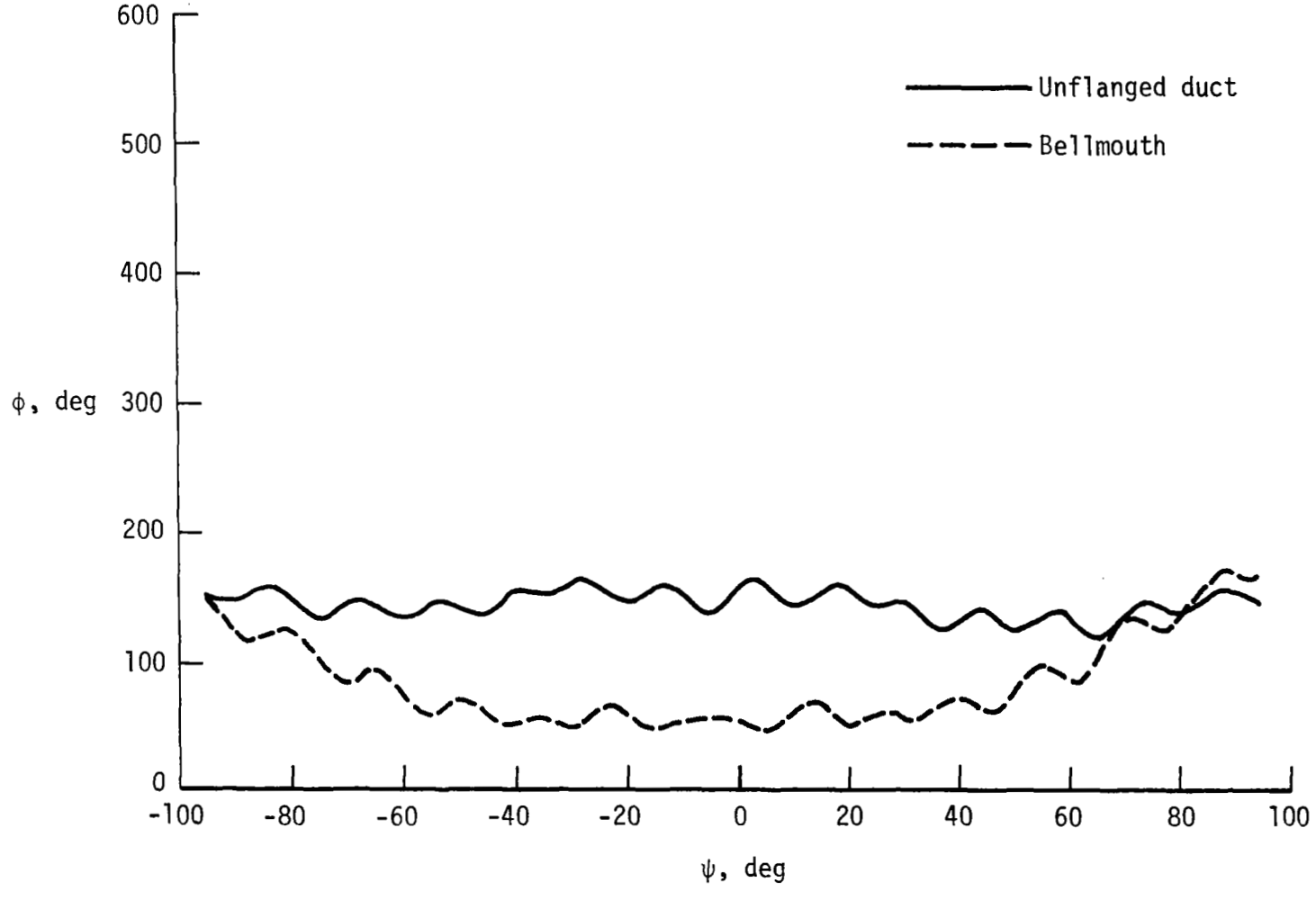

(a) Mode (0,0); ka = 1.39; M = 0.

Figure 21.- Influence of inlet geometry on phase variation of radiated field against polar angle.

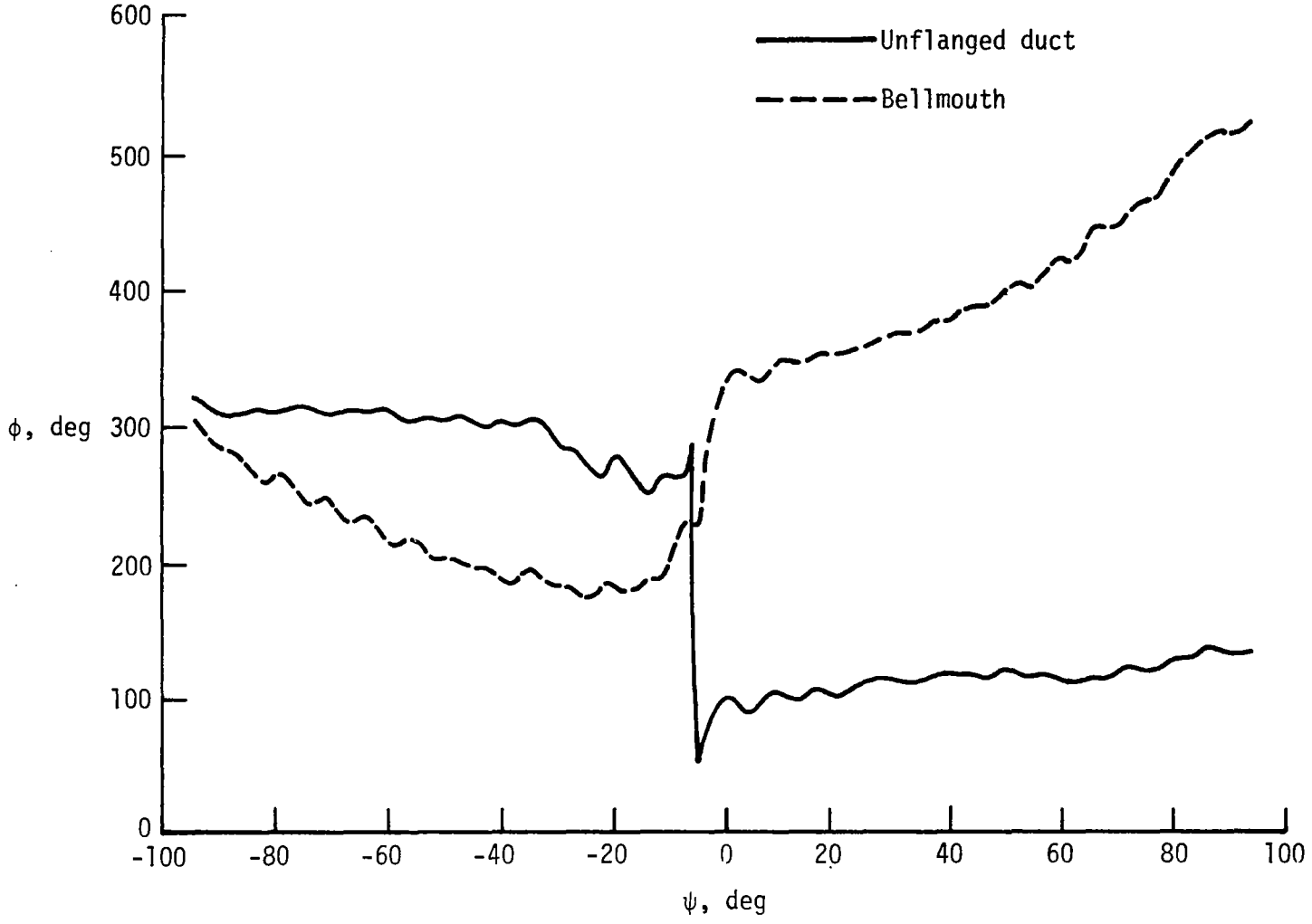

(b) Mode (1,0); ka = 2.66; f/f_{mn} = 1.44; M = 0.

Figure 21.- Concluded.

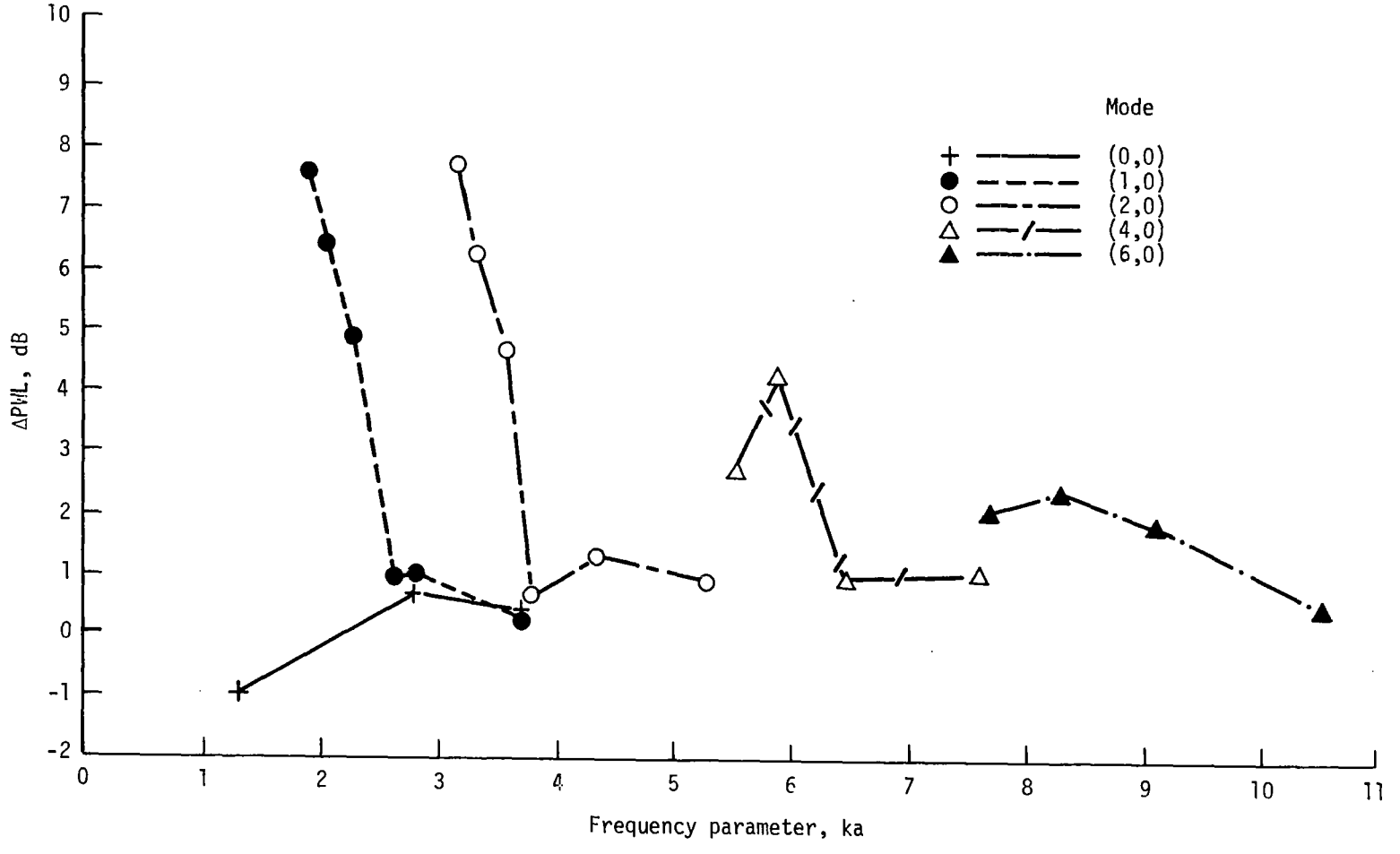

Figure 22.- Influence of inlet geometry on acoustic radiated power, measured samples; M = 0.

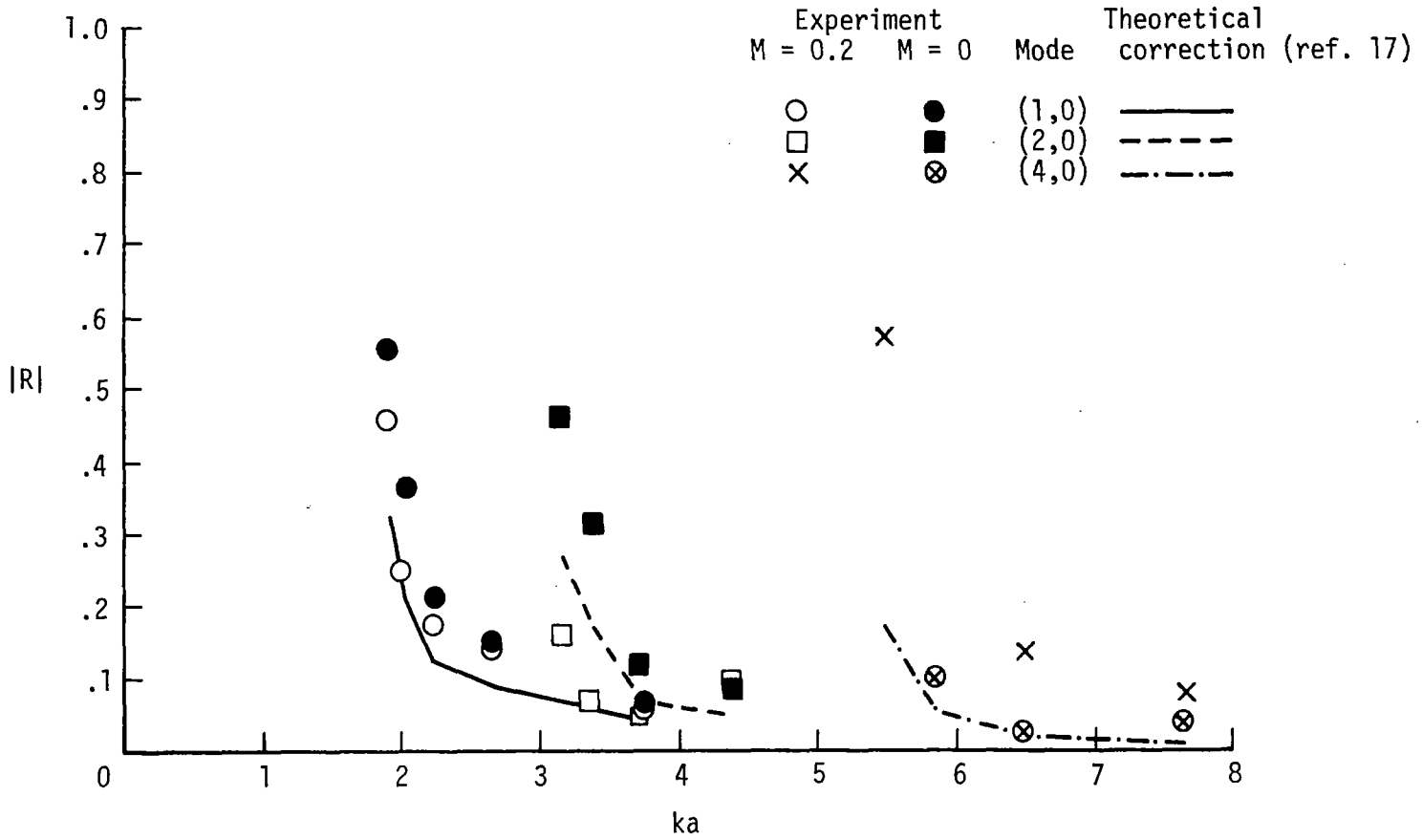

(a) Pressure reflection coefficient moduli.

Figure 23.- Influence of flow on pressure reflection coefficients for bellmouth and comparison with theoretical correction of reference 17.

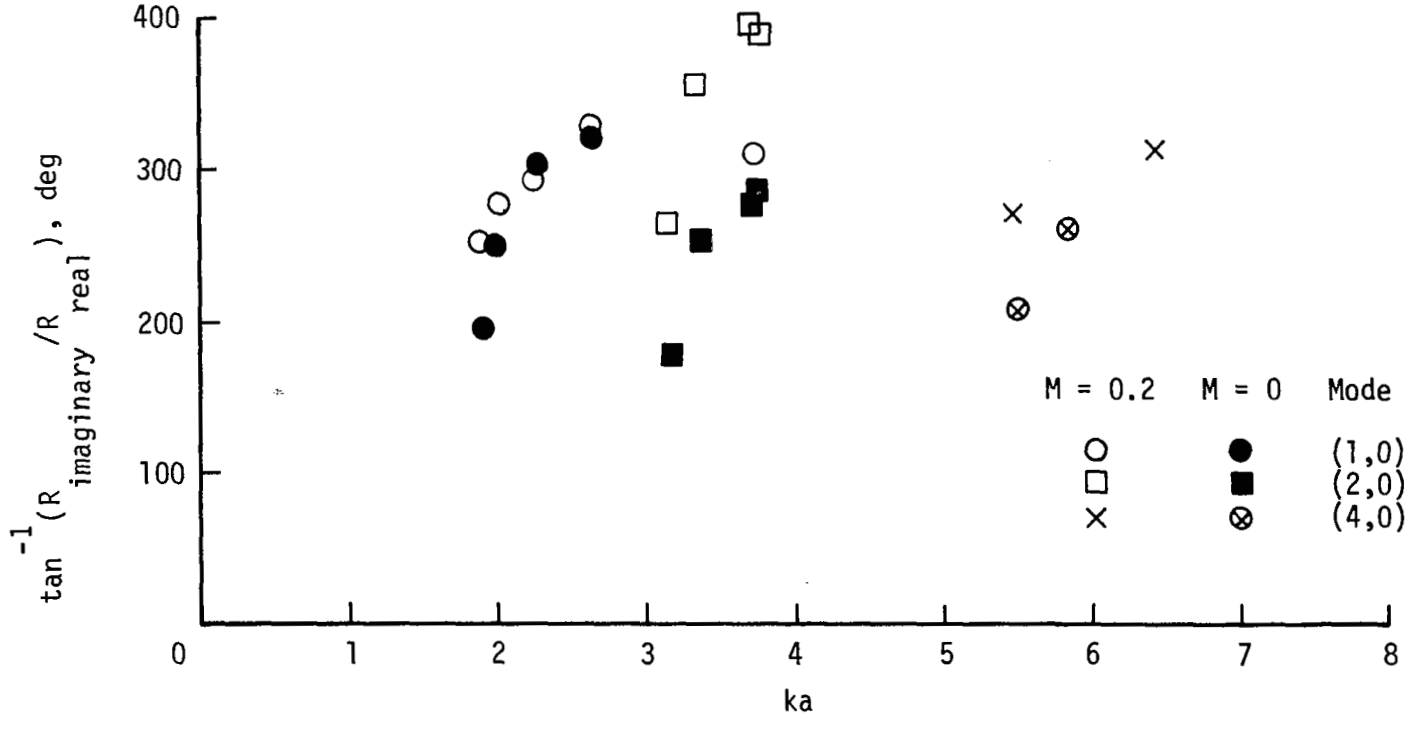

(b) Pressure reflection coefficient phase.

Figure 23.- Concluded.

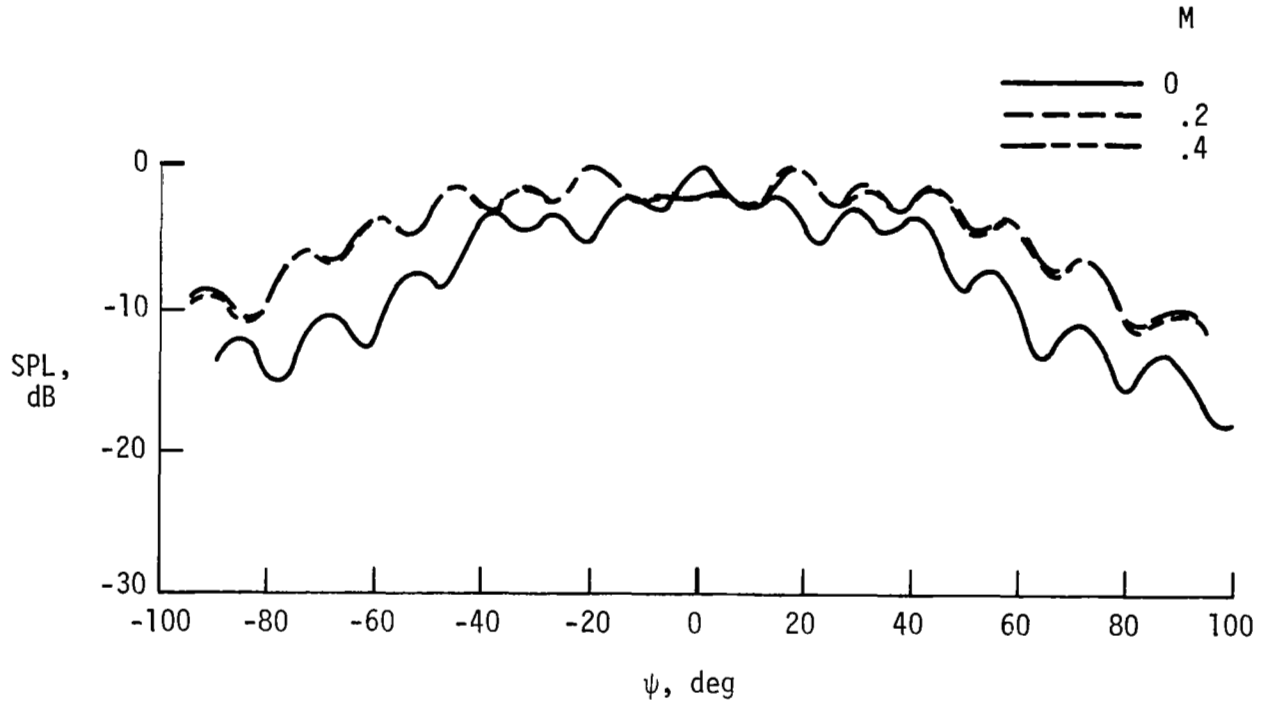

(a) Mode (0,0); ka = 1.39.

Figure 24.- Influence of flow on sound pressure level variation of radiated field against polar angle for bellmouth.

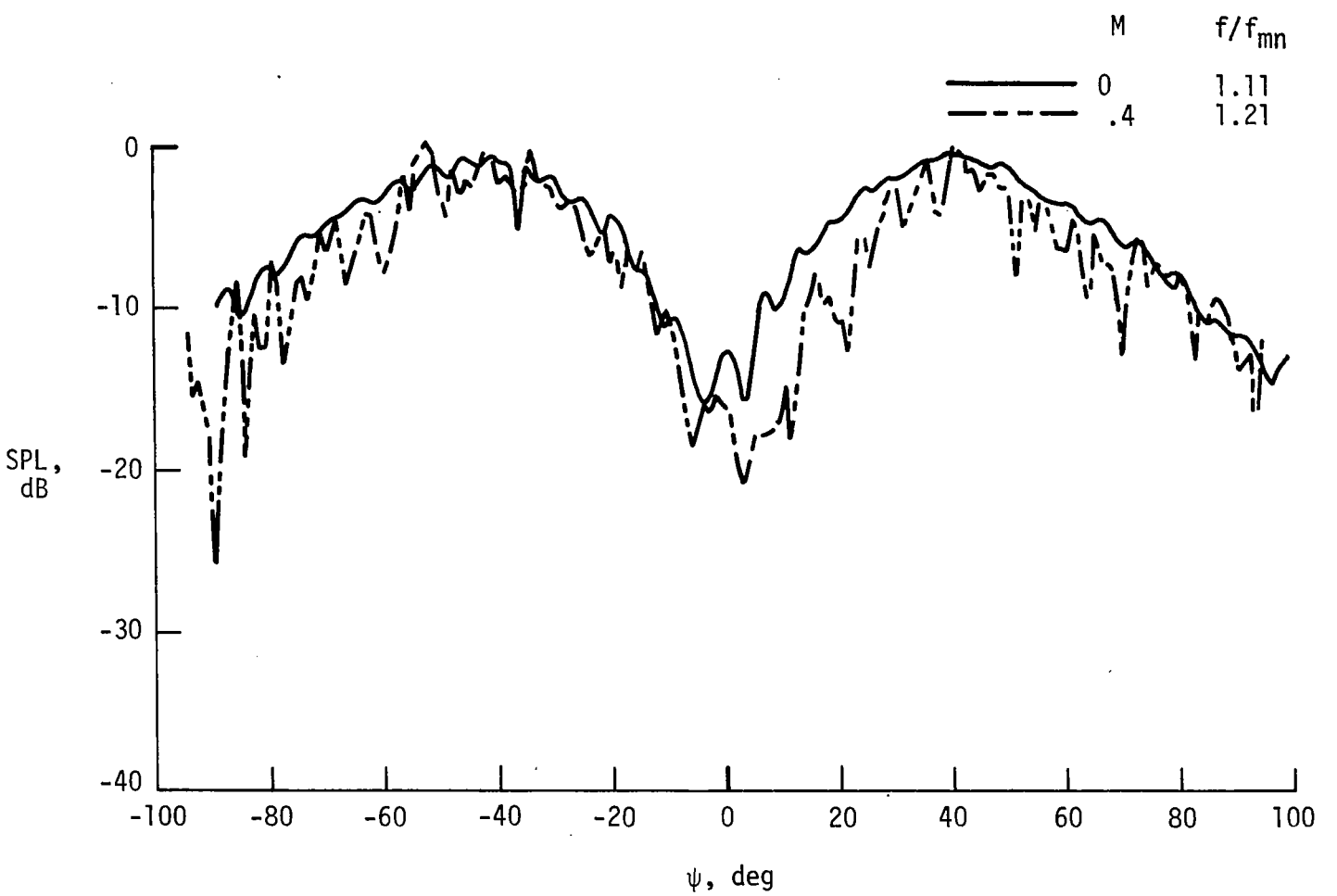

(b) Mode (2,0); ka = 3.37.

Figure 24.- Continued.

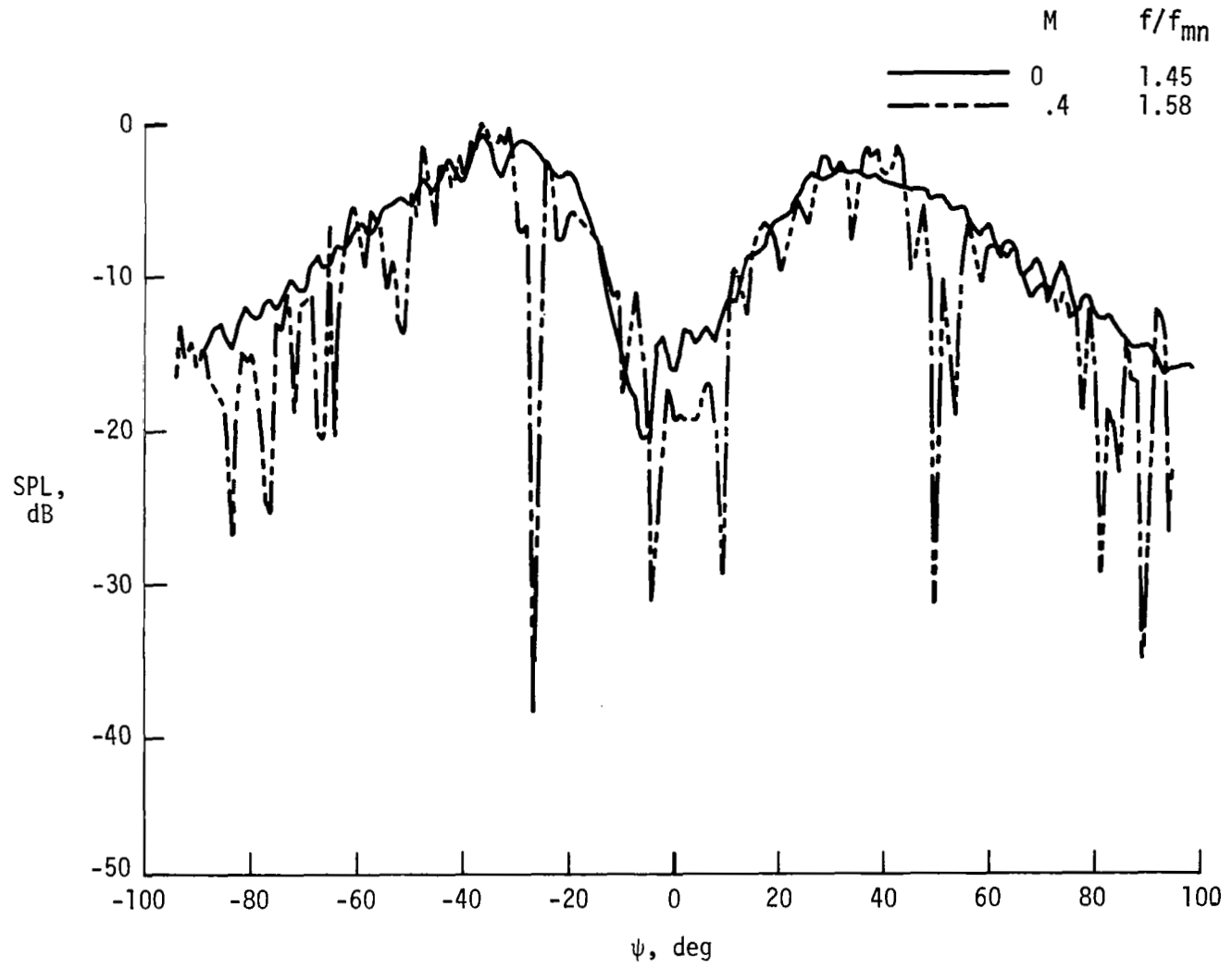

(c) Mode (2,0); ka = 4.4.

Figure 24.- Continued.

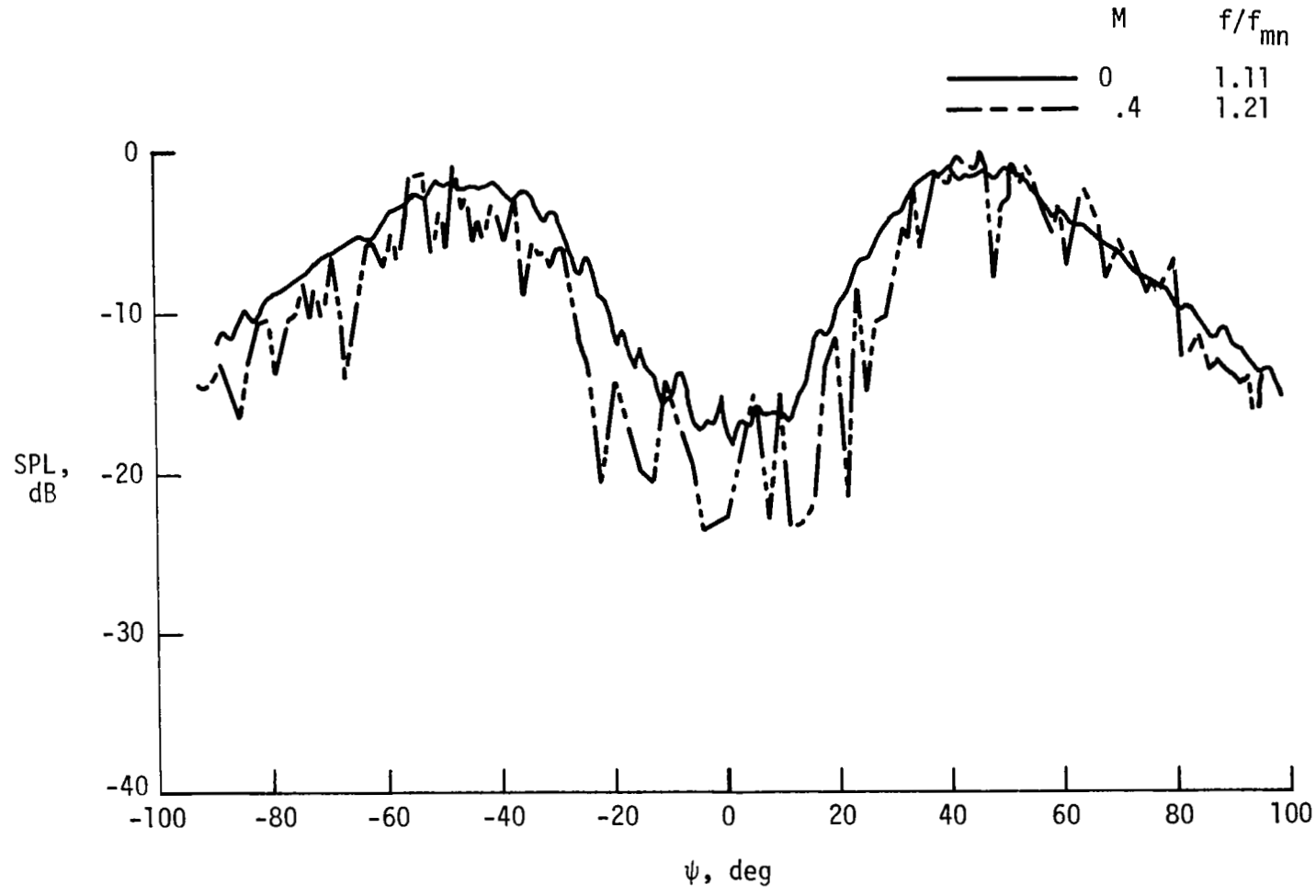

(d) Mode (4,0); ka = 5.81.

Figure 24.- Concluded.

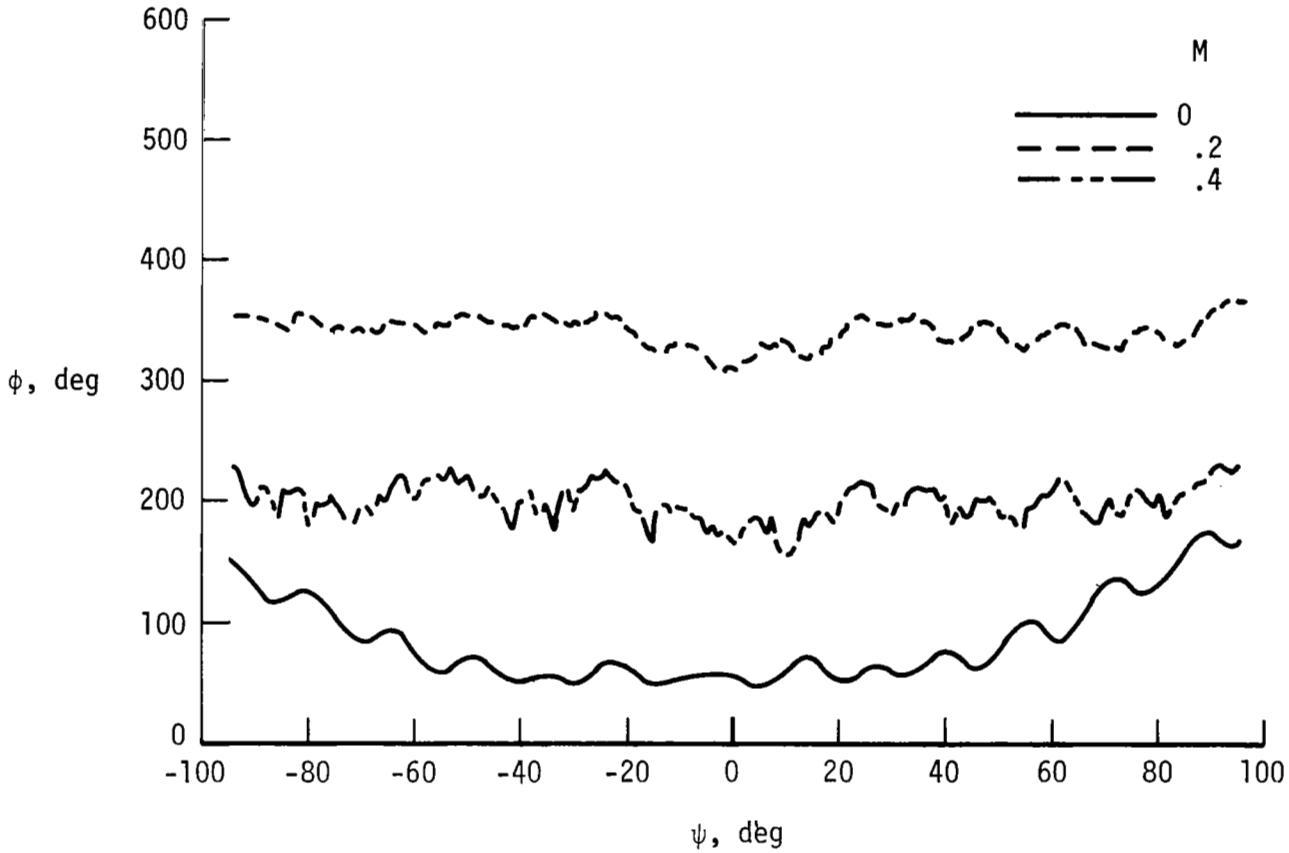

(a) Mode (0,0); ka = 1.39.

Figure 25.- Influence of flow on phase variation of radiated field against polar angle for bellmouth.

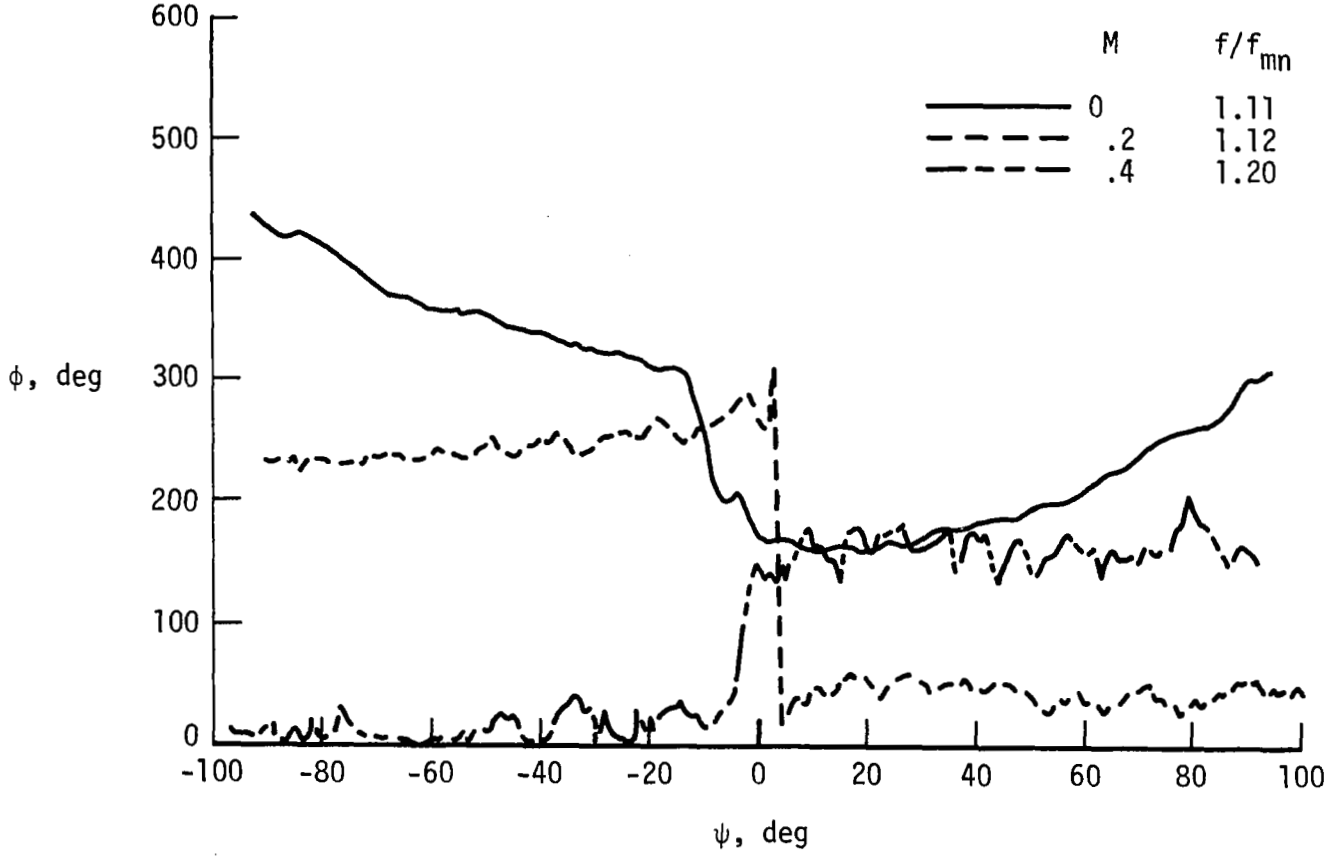

(b) Mode (1,0); ka = 2.03.

Figure 25.- Concluded.

1. Report No.	2. Government Accession No.	3. Recipient's Catalog No.
NASA TP-1697		

4. Title and Subtitle	5. Report Date
EXPERIMENTAL INVESTIGATION OF THE RADIATION OF SOUND FROM AN UNFLANGED DUCT AND A BELLMOUTH, INCLUDING THE FLOW EFFECT	August 1980
	6. Performing Organization Code
7. Author(s)	8. Performing Organization Report No.
Jean-Michel Ville and Richard J. Silcox	L-13252
	10. Work Unit No.
9. Performing Organization Name and Address	505-32-03-06
NASA Langley Research Center Hampton, VA 23665	11. Contract or Grant No.
	13. Type of Report and Period Covered
12. Sponsoring Agency Name and Address	Technical Paper
National Aeronautics and Space Administration Washington, DC 20546	14. Sponsoring Agency Code

15. Supplementary Notes

Jean-Michel Ville: Postdoctoral research associate with George Washington University, Joint Institute for Advancement of Flight Sciences; now at Université de Technologie de Compiegne, Compiegne, France.

16. Abstract

An experimental study of the radiation of sound from an inlet as a function of flow velocity, frequency, duct mode structure, and inlet geometry has been conducted by using a spinning mode synthesizer to insure a given space-time structure inside the duct. Measurements of the radiation pattern (amplitude and phase) and of the pressure reflection coefficient have been obtained over an azimuthal wave number range of 0 to 6 and a frequency range up to 5000 Hz for an unflanged duct and a bellmouth. The measured radiated field and pressure reflection coefficient without flow for the unflanged duct agree reasonably well with theory. The influence of the inlet contour appears to be very drastic near the cut-on frequency of a mode and reasonable agreement has been found between the bellmouth pressure reflection coefficient and a infinite hyperboloidal inlet theory. This investigation has also shown that the flow has a weak effect on the amplitude of the directivity factor but significantly shifts the directivity factor phase. The influence of the flow on the modulus of the pressure reflection coefficient has been found to be well described by a theoretical prediction.

17. Key Words (Suggested by Author(s))	18. Distribution Statement
Duct propagation Acoustic radiation Engine inlets	Unclassified - Unlimited Subject Category 71

19. Security Classif. (of this report)	20. Security Classif. (of this page)	21. No. of Pages	22. Price
Unclassified	Unclassified	62	A04

For sale by the National Technical Information Service, Springfield, Virginia 22161

NASA-Langley, 1980

6 1 1U,H, 081580 S00903DS
DEPT OF THE AIR FORCE
AF WEAPONS LABORATORY
ATTN: TECHNICAL LIBRARY (SUL)
KIRTLAND AFB NM 87117